People's **D**emocratic **R**epublic of **A**lgeria

Ministry of **H**igher **E**ducation and **S**cientific **R**esearch

University 20 august 1955 -skikda

Faculty of Sciences

Department of Physics

N° : .....

Master's Thesis

Field of Study: Physique

Speciality: Materials physics

Theme

Synthesis and Characterization of Mg-Doped SnS Thin Films for Photovoltaic Applications

Presented by:

Chebel Mouna

Defended on: 1/07/2025 before the jury composed of :

Kenza Kamli	MCA	University of Skikda	President
Zkaria Hadef	MCA	University of Skikda	Rapporteur
Nacira SASSANE	MRA	URMM, Annaba	Co- Rapporteur
Samira LALOUA	MCB	University of Skikda	Examiner

2024/2025


بسم الله الرحمن الرحيم

Acknowledgements

At the outset, I bow my head before the Almighty **ALLAH**, the Lord of the worlds, who endowed me with the enough vehemence to complete the task. Words are not enough to praise and thank for all the things given.

I would like to express my sincere thanks and deep appreciation to my supervisor, **Dr**. **Hadef Zkaria**, Professor at University of Skikda, for his invaluable support, continuous guidance, and constructive advice throughout the different stages of this work.

I am honored to thank the President of the jury, **Dr**. **Kenza Kamli**, Professor at University of Skikda, for accepting to chair the defense committee. I truly appreciate this gesture and the academic value it represents.

My sincere thanks also go to the Co-Rapporteur, **Dr**. **SASSANE Nacira**, Professor at the Mining and Metallurgy Research Unit (URMM) in Annaba, for her valuable time and for accepting to be involved in the assessment of this research work.

I am also grateful to the Examiner, **Dr**. **Samira LALOUA**, Professor at University of Skikda, for accepting to be a member of the jury and for agreeing to review and assess this research work.

Finally, I extend my heartfelt gratitude to everyone who has supported and encouraged me directly or indirectly throughout this journey.

Dedication

All praise is due to **Allah**, who guided me, granted me strength, and blessed me with the perseverance to complete this work. Without His mercy and guidance, none of this would have been possible.

I dedicate this humble work to my beloved parents.
To **my father**, for his wise words, his constant support, and the pride he instills in me every single day.
To **my mother**, for her boundless love, her unwavering belief in me, and for teaching me that nothing is impossible.
Thank you for everything you have given me.

To my two brothers, **Abd Raouf** and **Seif Eddine**, whose presence has always brought me comfort and motivation.

To my beloved uncle **Kamel**, who has always been like a second father to me, a true pillar throughout my life. Thank you from the bottom of my heart for your unconditional support, your reassuring presence, and your sincere love.

I would like to express my heartfelt gratitude to Ms **Lamiri Hayat** for her valuable support and kind assistance throughout this academic year. Her dedication and understanding have played a vital role in my success and in the completion of this work.

I sincerely thank my respected teacher Ms **Khelifi Ifrikia**, for her support and valuable guidance throughout my academic journey.
Her encouragement and insightful advice have always been a source of motivation, helping me overcome challenges and grow both academically and personally.

To my dearest friends: **Imane**, **Amel, Soussane**, **Roumaissa**, **Ibtissem**, **Ilheme**, and **Rayane,** thank you for always being by my side, for your kindness, encouragement, and unwavering support

To all my family, thank you for your love, support, and constant encouragement.

To all my friends and teachers at university.

الملخص

تم استخدام تقنية التحلل الحراري بالرذاذ فوق الصوتي (USP) لترسيب أغشية رقيقة من كبريتيد القصدير النقي والمطعم بالمغنيسيوم (SnS: Mg) عند درجة حرارة 350C °، وذلك مع تغيير تركيز شوائب المغنيسيوم (2%، 4%، 6% و8%). أكدت أنماط حيود الأشعة السينية أن الأغشية تمتلك بنية بلورية معينية الشكل (Orthorhombic) وقد تم تحديد بعض المعاملات التركيبية مثل حجم البلورات الدقيقة، والإجهاد الميكروي، وكثافة العيوب البلورية. كما تم حساب فجوة الطاقة البصرية من خلال قياسات النفاذية، حيث أظهرت قيمة منخفضة بلغت 1.59 eV، مع قمة انبعاث قوية في طيف الفلورة الضوئية تم رصدها عند 421nm لتركيز 6% من المغنيسيوم. أكدت قياسات تأثير هول (Hall Effect) أن الأغشية تمتلك موصلية من النوع p ، وأظهرت مقاومية منخفضة جدا بلغت $1.58\times 10^{-2}\ \Omega\cdot cm$، مع حركة عالية للناقلات بلغت $21.54 cm^2/Vs$، وتركيز حاملات شحنة مرتفع جدا قدره $1.47\times10^{19}\ cm^{-3}$للغشاء المحتوي على 6% من المغنيسيوم.

الكلمات المفتاحية :كبريتيد القصدير(SnS) ، التطعيم بالمغنيسيوم، التحلل الحراري بالرذاذ فوق الصوتي، حيود الأشعة السينية، فجوة الطاقة البصرية، الفلورة الضوئية، تأثير هول، الموصلية من النوع p ، الأغشية الرقيقة.

Abstract

Ultrasonic spray pyrolysis (USP) technique has been used to deposit pure and magnesium (Mg) incorporation Tin Sulfide (SnS: Mg) thin films at 350 °C by varying the Mg impurities concentration (2%, 4%, 6% and 8%). X -ray diffraction patterns confirm the orthorhombic crystal structure of SnS: Mg thin films. Structural parameters such as crystallite size, micro strain and dislocation density were determinated. The optical band gap energy was determinates by measuring the transmission which showed a low value of 1.59 eV with a strong emission peak of photoluminescence spectra observed at 421 nm for 6% of Mg incorporation concentration. Hall Effect measurement confirms the p-type conductivity of the SnS: Mg film and presented a very low resistivity of 1.58×10^{-2} Ω cm with the high mobility of 21.54 cm^2/Vs and very high carrier concentration of 1.47×10^{19} cm^{-3} for 6 at. % of SnS: Mg thin film.

Keywords: Tin sulfide (SnS), magnesium doping, ultrasonic spray pyrolysis, X-ray diffraction, optical band gap, photoluminescence, Hall Effect, p-type conductivity, thin films.

Résumé

La technique de pyrolyse par pulvérisation ultrasonique (USP) a été utilisée pour déposer des couches minces de sulfure d'étain pur et dopé au magnésium (SnS : Mg) à une température de 350 °C, en faisant varier la concentration d'impuretés de magnésium (2 %, 4 %, 6 % et 8 %). Les spectres de diffraction des rayons X ont confirmé que les films SnS : Mg présentent une structure cristalline orthorhombique. Les paramètres structuraux tels que la taille des cristallites, la microcontrainte et la densité de dislocations ont été déterminés.

L'énergie de la bande interdite optique a été estimée à partir des mesures de transmission, révélant une faible valeur de 1,59 eV, avec un pic d'émission intense dans le spectre de photoluminescence observé à 421 nm pour une concentration de 6 % de magnésium. Les mesures de l'effet Hall ont confirmé la conductivité de type p du film SnS : Mg, en montrant une très faible résistivité de $1{,}58 \times 10^{-2}\ \Omega\cdot\text{cm}$, une mobilité élevée des porteurs de charge de $21{,}54\ \text{cm}^2/\text{Vs}$ et une concentration en porteurs très élevée de $1{,}47 \times 10^{19}\ \text{cm}^{-3}$ pour le film contenant 6 % de Mg.

Mots-clés : Sulfure d'étain (SnS), dopage au magnésium, pyrolyse par pulvérisation ultrasonique, diffraction des rayons x, bande interdite optique, photoluminescence, effect hall, conductivité de type p, couches minces.

Table of Contents

List of Figures

List of Tables

General introduction 1

Chapter I: Photovoltaic Technology and Thin Film Deposition Methods for Solar Applications

I.1. Introduction 5

I.2. Photovoltaic Technology 5

I.2.1. Definition 5

I.2.2. Principle of the Photovoltaic Effect 5

I.2.3. Photovoltaic Cell 6

I.2.3.1. Operation Principle of a Photovoltaic Cell 6

I.3. Overview of Thin Films 8

I.3.1. History of Thin-Film Development 8

I.3.2. Thin-Film Deposition and Growth Mechanisms 9

I.3.2.1. Principles of Thin-Film Deposition 9

I.3.2.1.a. The source 10

I.3.2.1.b. Transport 10

I.3.2.1. c. Deposition 11

I.3.2.1.d. Analysis 11

I.3.2.2. Mechanism of Thin Film Growth 11

I.3.2.2.a. Nucleation 11

I.3.2.2.b. Coalescence 12

I.3.2.2.c. Growth 12

I.4. Thin-Film Deposition Methods 12

I.4.1. Physical Deposition Methods 13

I.4.1.1. Physical Vapor Deposition (PVD) 13

I.4.1.1.a. Vacuum Evaporation 13

I.4.1.1.b. Laser Ablation 14
I.4.1.1.c. Sputtering Technique 15
I.4.2. Chemical Deposition Methods 15
I.4.2.1. Chemical Vapor Deposition (CVD) 15
I.4.2.1.a. Atomic Layer Deposition (ALD) 16
I.4.2.1.b. Thermal CVD 16
I.4.2.1.c. Plasma-Enhanced CVD (PECVD) 17
I.4.2.2 Sol-Gel Method 17
I.4.2.2.a. Spin-Coating (Centrifugation) 17
I.4.2.2.b. Dip-Coating 18
I.4.2.3 Spray Pyrolysis 20
I.5.Conclusion 21
References 22
Chapter II: Characterization and Preparation of Tin Sulfide (SnS) Thin Films
II.1. Introduction 28
II.2. Tin Sulfide (SnS) 28
II.2.1. Choice of SnS Material 28
II.2.2. Phase Diagram of the Sn-S System 29
II.3. Physical properties of SnS 30
II.3.1. Macroscopic Appearance of Tin Sulfide 30
II.3.2. Growth Mechanisms and Kinetics 30
II.3.3. Crystal Structure 31
II.3.4. Optical Properties of SnS 32
II.3.5. Electrical Properties of SnS 33
II.4. Experimental Techniques 34
II.4.1. Ultrasonic Spray Pyrolysis (USP) 34
II.4.1.1. Experimental Setup 34
II.4.1.2. Working Principle of Ultrasonic Spray Pyrolysis 34

II.4.2. X-ray Diffraction (XRD) 36
II.4.2.1. Principle 36
II.4.2.2. Bragg's Law 37
II.4.2.3. Determination of Crystallite Size 37
II.4.2.4. Experimental Setup 38
II.4.3. UV–Visible Spectrophotometry 38
II.4.3.1. Principle 39
II.4.4. Electrical Characterization by Hall Effect 40
II.5. SnS:Mg Films Prepared by Ultrasonic Spray Pyrolysis 41
II.5.1. Substrate Preparation 41
II.5.2. Precursor Solution Preparation 42
II.5.3. Ultrasonic Spray Deposition 43
II.6. Conclusion 43
References 44
Chapter III: Results and discussions
III.1. Introduction 48
III.2. Structural analysis 48
III.3. Optical analysis 52
III.4. Electrical properties 54
III.5. Conclusion 55
References 56
General Conclusion 58

List of Figures

Chapter I

Figure	Title	Page
Figure.I.1	Electricity Generation by Photoelectric Conversion.	6
Figure.I.2	Structure of a cell (on the left) and its band diagram (on the right)	7
Figure.I.3	Thin film deposition techniques.	12
Figure.I.4	Schematic of vacuum evaporation process with E-beam heating	13
Figure.I.5	Schematic of the PLD process	14
Figure.I.6	Sputtering system diagram	15
Figure.I.7	Principle of Atomic Layer Deposition (ALD)	16
Figure.I.8	Experimental Setup of PECVD.	17
Figure.I.9	Schematic illustration of the spin coating process	18
Figure.I.10	A graphical illustration of the dip coating technique	18
Figure.I.11	Overview showing two synthesis examples by the sol–gel method; (a) films from a colloidal sol; (b) powder from a colloidal sol transformed into a gel	19
Figure.I.12	Schematic representation of primary and secondary particles in alkoxide gel	20
Figure.I.13	Schematic Diagram of the Spray Pyrolysis Deposition Principle	20

Chapter II

Figure	Title	Page
Figure.II.1	Phase of the SnS system	29
Figure.II.2	Macroscopic appearance of tin sulfide	30
Figure.II.3	Variation of film thickness with substrate temperature	31
Figure.II.4	(a-d) crystal structure of various SnS polymorphs, (e) SnS_2 and (f) Sn_2S_3 (Sn and S in grey and yellow color, respectively)	32
Figure.II.5	Dependence of the transmittance versus the photon energy	32
Figure.II.6	Experimental ultrasonic spray setup	34

Figure.II.7	Schematic Diagram of the Ultrasonic Spray Pyrolysis System.	35
Figure.II.8	Principle of X-ray diffraction	36
Figure.II.9	Bragg's Law reflection	37
Figure. II.10	Illustration Showing the Definition of β from the X-ray Diffraction Curve	38
Figure. II.11	X-ray Diffractometer (Malvern PANalytical® Empyrean Series)	38
Figure.II.12	Schematic Representation of a UV-Visible Spectrophotometer	39
Figure. II.13	Perkin Elmer Lambda 950 UV-Vis spectrophotometer	39
Figure.II.14	Schematic Representation of the Hall Effect	40
Figure.II.15	Setup of the HMS 3000 Instrument Used for Electrical Characterization	41
Figure.II.16	Experimental steps for preparing the magnesium-doped precursor solution	42

Chapter III

Figure	Title	Page
Figure.III.1	XRD patterns of pure and SnS: Mg thin films	48
Figure.III.2	Variation of crystallite size and Strain of pure and SnS: Mg thin films	51
Figure.III.3	Transmission spectra of SnS: Mg samples	52
Figure.III.4	Variation of $(\alpha h\nu)^2$ as a function of the photon energy ($h\nu$)	53
Figure III.5	Variation of Resistivity and Conductivity with Mg Incorporation in SnS Thin Films	54

List of Tables

Chapter II

Table	Title	Page
Table.II.1	The optical band gap of SnS material by different techniques	33
Table.II.2	Summarizes the electrical properties of SnS films prepared using various deposition techniques	33

Chapter III

Table	Title	Page
Table.III.1	Microstructural parameters of pure and SnS: Mg thin films	51
Table.III.2	Summarizes values of electrical proprieties of pure and SnS: Mg thin films	54

General introduction

General introduction

Solar photovoltaic (PV) technology is one of the most promising renewable energy sources for creating a clean, reliable, and affordable electricity supply. Achieving cost-effective thin-film solar cells for large-scale energy requires the use of semiconductor absorber materials that are inexpensive, non-toxic, and abundant. Furthermore, these materials must possess suitable optical and electrical properties such as an optimal band gap, high absorption coefficients, efficient carrier generation, and low recombination rates to ensure high energy conversion efficiency. [1]

SnS has emerged as a promising semiconductor for photovoltaic applications due to its non-toxicity, low cost, and good stability [2,3,4]. It is a naturally p-type semiconductor with excellent optoelectronic properties and can be processed at relatively low temperatures, which improves manufacturing efficiency and allows for the deposition on flexible substrates.

Crystalloraphically, SnS has an orthorhombic layered structure, where atoms are strongly bonded within layers and weakly bonded between them, resulting in anisotropic carrier transport [5]. Its intrinsic p-type conductivity mainly arises from tin vacancies in the crystal lattice [6].

Taking into consideration such favorable properties, SnS-based solar cell performance is below theoretical expectation due to phase purity issues, low carrier mobility, and intrinsic defects. Conventional doping strategies have been explored to mitigate the limitations mentioned above and thus improve the structural, optical, and electrical properties of SnS thin film.

In this context, the present work focuses on the synthesis and characterization of magnesium-doped SnS (SnS: Mg) thin films, deposited using ultrasonic spray pyrolysis (USP) a simple, scalable, and low-cost chemical deposition technique. The aim is to optimize the deposition parameters to improve film quality and investigate the effects of Mg doping on the structural, optical and electrical characteristics of SnS with a view toward photovoltaic applications.

Therefore, the thesis is divided as follows. Chapter One provides a general overview of photovoltaic technologies, the physical principles of solar energy conversion, and a detailed review of thin -film deposition methods used in solar cell fabrication.

Chapter Two discusses the theoretical background and experimental details related to SnS thin films, including the motivation for using SnS, its fundamental properties, the characterization technique employed and the step-by-step synthesis of Mg-doped SnS films using USP.

Chapter Three presents the experimental results and discusses the influence of Mg doping on the structural, optical and electrical behavior of SnS thin films. The findings are analyzed in the context of their potential use in photovoltaic applications.

This study aims to contribute to the advancement of efficient and low-cost photovoltaic materials by exploring the potential of Mg-doped SnS thin films, thereby bridging the gap between laboratory scale research and scalable real-world applications.

References

[1] R. Bube, "Photovoltaic Materials", Series on Properties of Semiconductor Materials, 1, Imperial College Press, London, (1998).

[2] L. Price, I. Parkin, A. Hardy, R. Clark, "Atmospheric pressure chemical vapor deposition of tin sulfides (SnS, Sn_2S_3, and SnS_2) on glass", Chemistry of Materials, Vol.11 (1999) 1792–1799.

[3] P. Sinsermsuksakul, J. Heo, W. Noh, A. Hock, R. Gordon, "Atomic layer deposition of tin monosulfide thin films", Advanced Energy Materials, Vol.1 (2011) 1116–1125.

[4] L. Burton, T. Whittles, D. Hesp, W. Linhart, J. Skelton, B. Hou, et al., "Electronic and optical properties of single crystal SnS_2: An earth-abundant disulfide photocatalyst", Journal of Materials Chemistry A, Vol.4 (2016) 1312–1318.

[5] S. Sucharitakul, U. Kumar, R. Sankar, F. Chou, Y. Chen, C. Wang, et al., "Screening limited switching performance of multilayer 2D semiconductor FETs: The case for SnS", Nanoscale, Vol.8 (2016).

[6] Y. Kumagai, L. Burton, A. Walsh, F. Oba, "Electronic structure and defect physics of tin sulfides: SnS, Sn_2S_3, and SnS_2", Physical Review Applied, Vol.6 (2016).

Chapter I:

Photovoltaic Technology and Thin Film Deposition Methods for Solar Applications

I.1. Introduction

Photovoltaic technology has become one of the most promising solutions for sustainable energy production, allowing the direct conversion of sunlight into electricity through the Photovoltaic effect. With growing global demand for clean energy, research and innovation in PV materials and devices have accelerated. This chapter introduces the basic concepts of photovoltaic technology, including its definition, working principle and the structure and operation of photovoltaic cells. It then provides an overview of thin-film technology, outlining its historical development, deposition principles and growth mechanism. Finally, the chapter presents various thin-film deposition methods, both physical and chemical, highlighting the advantages and applications of each in photovoltaic device fabrication.

I.2. Photovoltaic Technology

I.2.1 Definition

The term " photovoltaic " is derived from of the word « photo » meaning light and " voltaic " which comes from the name of volta, the discoverer of the electric battery. It refers to the conversion of solar radiation into electricity.

Therefore, photovoltaic energy describes the process of transforming light energy into electricity through solar cells and photovoltaic modules. this conversion occurs through a phenomenon Knows as the " photovoltaic effect " [1].

I.2.2 Principle of the Photovoltaic Effect

Photovoltaic conversion can be simply defined as the transformation of photon energy into electrical energy through the process of light absorption by matter. when a photon is absorbed by the material, it transfers part of its energy through a collision to an electron, effectively extracting it from the material. This electron, previously at a lower energy level in a stable state, moves to a higher energy level, creating an electrical imbalance within the material, which results in an electron -hole pair of the same electrical energy [2].

This phenomenon , known as the photovoltaic effect ,generates an electromotive force when the surface of a photovoltaic cell is exposed to light .The voltage produced typically ranges between 0.3 V and 0.7 V , depending on factors such as the material used , its structural arrangement , the temperature and the aging of the cell [3].This process is made possible by solar cells formed by combining an N-doping semiconductor with a p-doped semiconductor .

I.2.3 Photovoltaic Cell

The PV cell, also known as a photo pile is the smallest element of a photovoltaic installation. it is made of semiconductor materials and directly converts light energy into electrical energy. Photovoltaic cells consist of:

- A thin semiconductor layer (a material with a band gap, which acts as an energy barrier that electrons cannot cross without external excitation, and whose electronic properties can be modified) such as silicon, which is a material with relatively good electrical conductivity.
- An anti-reflective layer allowing maximum penetration of solar rays.
- A conductive grid on the top, known as the cathode, and a conductive metal on the bottom, known as the anode.

The most recent cells even include a new combination of reflective multilayers just below the semiconductor, allowing light to bounce for a longer time within the material to improve efficiency.[4]

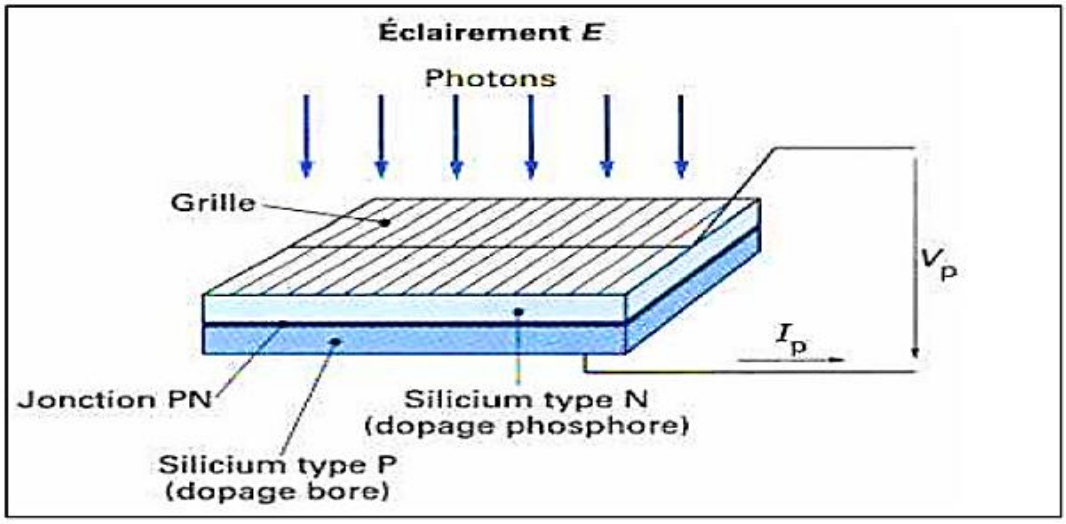

Figure I.1: Electricity Generation by Photoelectric Conversion [5]

I.2.3.1. Operation Principle of a Photovoltaic Cell

A photovoltaic cell is a device that converts solar energy directly into electrical energy. This conversion is based on the following three fundamental mechanism:

- ✓ **Photon absorption:** photons with energy greater than the band gap are absorbed by the semiconductor material that constitutes the cell.

- ✓ **Energy conversion:** The absorbed photon energy is transformed into electrical energy through the generation of electron-hole pairs within the semiconductor material.
- ✓ **Charge carrier collection:** The generated charge carriers (electrons and holes) are separated and collected to produce an electric current.

For a photovoltaic cell to function efficiently, the material must have two well-defined energy levels and possess sufficient electrical conductivity to allow the flow of electric current. These properties make semiconductors the most suitable materials for photovoltaic applications. The separation of electron-hole pairs requires the presence of an electric field. This is typically achieved using a PN junction, which is the most commonly employed structures. However, other configuration, such as heterojunction and Schottky junctions, can also be utilized to enhance performance and efficiency. The operating principle of photovoltaic cells is illustrated in Figure I.2.

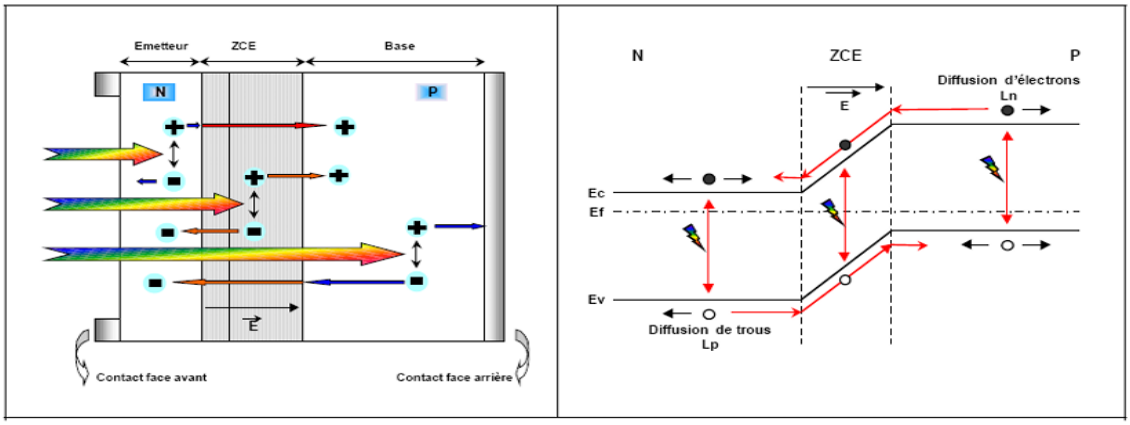

Figure I.2: Structure of a cell (on the left) and its band diagram (on the right).

When incident photons strike the photovoltaic cell, they generate charge carriers in the N and P regions as well as in the depletion region. The behavior of these photogenerated carriers depending on the region where they are created:

In the N or P regions: Minority carriers that reach the depletion region are driven by the electric field towards the P region (for holes) or the N region (for electrons), where they become majority carriers. This process results in the formation of diffusion photocurrent.

In the depletion region: Electron-hole pairs generated by incident photons are separated by the electric field: electrons migrate toward the N region, while holes move toward the P region. This separation leads to the generation or drift photocurrent [6].

I.3. Overview of Thin Films

Thin films are thin layers of materials with thicknesses ranging from nanometers to several micrometers, applied to the surface of target materials to introduce new properties that were not previously present. This technique is extensively used in the fabrication of semiconductors, optical coatings and anti-reflective layers [7,8].

A key advantage of thin films lies in their efficient use of materials while preserving essential physical properties, as well as the simplicity and cost-effectiveness of the technologies used for their fabrication. A wide range of materials can be utilized to produce thin films, including metals, alloys, refractory compounds, and polymers. One fundamental characteristic of thin films is that, regardless of the manufacturing methos, they are always bonded to a substrate on which they are formed. In certain cases, it is possible to separate the thin film from the substrate.

It is essential to recognize that the substrate plays a critical role in determining the structural properties of the deposited layer. For example, a thin film of the same material and thickness may exhibit significantly different physical properties depending on whether it is deposited on an amorphous insulating substrate, such as glass, or a monocrystalline silicon substrate. As a result of these defining characteristics, thin films are inherently anisotropic by nature [9].

The primary distinction between bulk materials and thin films lies in the influence of surface boundaries .In bulk materials , surface effects on physical properties are generally negligible .In contrast , thin films are predominantly affected by surface boundaries .The thinner the film , the more pronounced the two-dimensional effects become .Conversely , when the thickness exceeds a certain threshold ,these effects diminish ,and the material regions the well-known properties of its bulk form [10].

I.3.1 History of Thin-Film Development

Thin-film technology is both one of the oldest practical and one of the most advanced modern sciences [11]. The use of thin films dates back to the meatal ages of antiquity. An early example is the ancient practice of gold beating, which has been used for at least four millennia. Gold is highly malleable, allowing it to be hammered into very thin sheets. Its beauty and resistance to chemical degradation made it useful for decoration and protection [12].

The concept of nanotechnology was introduced by Richard Feynman during a 1959 meeting of the "American Physical Society". The term "nanotechnology" was first used by Norio Taniguchi from the Tokyo university of science in 1974.He defined it as "the processing, separation, consolidation and deformation of materials by one atom or molecule" [13].

In the 1980s, Eric Drexler highlighted the importance of nanoscale materials and phenomena. During this time, new experimental technique advanced nanotechnology. The scanning tunneling microscope (STM) was invented in 1981 by Gerd Binnig and Heinrich Rohrer. They received the Nobel Prize in Physics in 1986.In 1986, Calvin F. Quate and Christopher Gerber invented the atomic force microscope (AFM). These tools allowed scientists to observe and manipulate individual atoms and molecules.

Transmission electron microscope (TEM) and scanning electron microscopy (SEM) are also used to study nanomaterials. Ernst Ruska was awarded the Nobel Prize in physics in 1928 for building the first electron microscope in 1928.In 1933 he achieved the first observation with a resolution higher than an optical microscope. In recent years. the "top-down" approach has become an essential method in nanotechnology. This method allows the creation of small structures by cutting or shaping larger materials [14].

I.3.2 Thin-Film Deposition and Growth Mechanisms

I.3.2.1 Principles of Thin-Film Deposition

To form a thin film on a solid surface (substrate), the particles of the coating materials must pass through a conductive medium until they come into direct contact with the substrate. Upon reaching the substrate, a portion of the coating particles adheres through Van der walls forces or undergoes chemical reaction with the substrate. These particles can be atoms, molecules, ions or fragments of ionized molecules. The transport medium can be solid, liquid, gas or vacuum.

In the case of Solid medium, the substrate is in direct contact with the solid and only the particles that diffuse from the solid to the substrate contribute to forming the thin film. However, achieving thin films through solid-solid contact is generally challenging. For instance, oxygen diffusion from silica can form a thin SiO_2 layer on a silicon substrate.

The Liquid medium offers more feasibility than the solid-state method due to the greater versatility of materials in the liquid phase (e.g. electrochemical deposition, and sol-gel methods).

In Gas or vacuum media such as in Chemical Vapor Deposition (CVD), the primary difference between the gaseous medium and the vacuum lies in the mean free path of the particles. There is no universal thin-film deposition method applicable to all scenarios. Proper substrate preparation is often a critical step to ensure strong adhesion of the thin film [15].

I.3.2.1. a. The source

The source represents the base material for the thin film to be developed .it can be a solid, liquid, vapor, or gas. When the material is solid, its transport to the substrate occurs through vaporization. this can be achieved by thermal evaporation, electron beam, laser ablation, or positive ion bombardment (sputtering). These methods are collectively known as Physical Vapor Deposition (PVD).

Occasionally, the solid source is converted into vapor through chemical reaction .in other cases, the base material exists as a gas or a liquid with sufficient vapor pressure to be transported at moderate temperatures. Processes that use gases, evaporated liquids, or chemically evaporated solids as the base material are known as chemical Vapor Deposition (CVD) [16].

I.3.2.1. b. Transport

During the transport stage, the uniformity of the species flux arriving at the substrate surface is a critical factor. several factors affect this uniformity, depending on the transport medium, which can be a high vacuum or a fluid (mainly gases). In a high vacuum, the molecules travel in straight lines from the source to the substrate without collisions. In contrast, in a fluid medium, the molecules undergo multiple collisions during their transport.

In vacuum-based processes, the flux uniformity is determined by the system's geometry, while in a fluid medium, it depend on the gas flow rate and the diffusion of source molecules among other gases. Typically, processes operating in high vacuum correspond to PVD method, while those involving fluid flow are classified as CVD methods. However, this distinction is not always absolute.

Some PVD processes operate in high vacuum, while others, such as laser ablation and sputtering, often function at higher pressures typical of fluid environments. Similarly, most CVD processes operate at moderate pressures. Many thin-film deposition processes utilize a plasma environment. The high energy within plasma enables the activation of thin-film

formation at low temperatures. The working pressure of a plasma can be similar to that of a fluid [17].

I.3.2.1. c. Deposition

The third step in thin -film deposition processes is the deposition of the film onto the substrate surface. This stage involves nucleation and coalescence processes. The deposition behavior is determined by the source; transport condition and three primary factors related to the substrate surface:

1. Surface condition (roughness, contamination level, chemical potential with the incoming material).

2. Reactivity of the incoming material on the surface (sticking coefficient).

3. Energy delivered to the surface (substrate temperature, photon energy, positive ion bombardment) [18].

I.3.2.1. d. Analysis

The final stage in the thin-film fabrication process is the analysis of the deposited film. The first level of material evaluation involves direct measurement of its essential properties. If these results are insufficient, additional specialized experiments are required to resolve any ambiguities in the process [19].

I.3.2.2. Mechanism of Thin Film Growth

All thin film processes occur in three stages:

a) Generation of appropriate ionic, molecular, or atomic species.

b) Transport of these species to the substrate.

c) Condensation on the substrate, involving nucleation, coalescence, and growth.

I.3.2.2.a. Nucleation

The sputtered species arriving at the substrate are not in thermodynamic equilibrium with it and move across its surface. In this state, they interact with each other and form what are called "clusters". Under specific deposition condition these clusters collide with other adsorbed species and begin to grow. upon reaching a critical size, these clusters become thermodynamically stable, marking the point where the nucleation barrier is overcome [20,21].

I.3.2.2.b. Coalescence

The coalescence process occurs is two stages. the first stage Involves the growth of stable islands through the absorption of smaller clusters by larger ones. This stage is followed by a faster, large-scale coalescence, where the islands, having reached a critical density, flatten to increase their surface coverage and merge with neighboring islands.

If the probability of all islands on the substrate being oriented in the same direction is low, the coalescence results in a polycrystalline deposit. conversely, if the islands share the same orientation, a thin monocrystalline layer develops [22].

I.3.2.2.c. Growth

During the growth stage, the islands begin to aggregate into larger structures. This tendency to form larger islands is enhanced by increasing the surface mobility of the adsorbed species, which can be achieved by raising the substrate temperature. As these larger islands continue to grow, they leave channels and voids on the substrate.

At this stage, the film structure transitions from discontinuous islands to a porous network. A continuous film forms as the channels and voids gradually fill [20].

I.4. Thin-Film Deposition Methods

There are several techniques used for thin-film deposition, which can be classified into two main categories: Physical Deposition Methods and Chemical Deposition Methods, as illustrated in Figure I.3 [22]. This classification is based on the nature of the deposition process and is fundamental for understanding the various methods employed in the fabrication of thin films and their diverse applications.

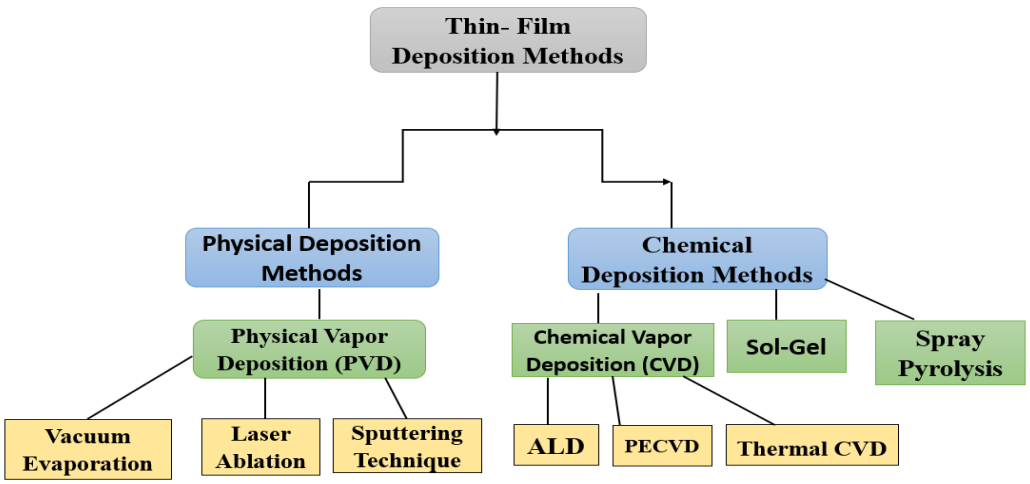

Figure I.3: Thin film deposition techniques.

I.4.1 Physical Deposition Methods

I.4.1.1 Physical Vapor Deposition (PVD)

Physical Vapor Deposition (PVD) is a broad class of techniques for depositing thin films (evaporation, laser ablation and various forms of sputtering). Although all these several techniques have different steps, there are three basic processes involved in them according to [23]:

• Vaporization of the material to be deposited.

• Transporting the vaporized material from the source to the substrate.

• The deposition of the vapor on the surface of the substrate to form a thin film.

This technique is widely used due to the ability to produce thin films of very high purity, uniform thickness and excellent adhesion, which are important for application in electronics, optics and surface protection.

I.4.1.1.a. Vacuum Evaporation

Vacuum evaporation is a thin-film deposition method that involves the condensation of vaporized material onto a substrate to form coating. The vapor is generated by heating the source material [24]. There are a number of heating methods to produce evaporation, including electrical heating with the help of a resistance element (Joule effect), magnetic field induction, electron beam, laser beam or electric arc,

the material to be deposited is placed in a crucible, typically made of tungsten. This method is particularly suitable for metallic as evaporation temperature of the metal is lower than the melting point of the crucible. Figure I.4 shows the basic principle of this process [25].

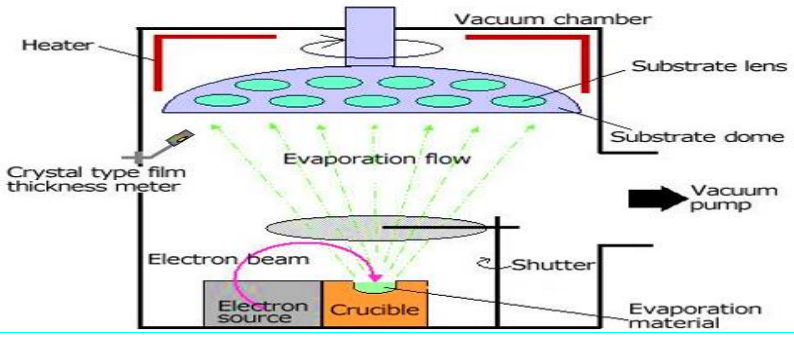

Figure I.4: Schematic of vacuum evaporation process with E-beam heating [26]

I.4.1.1.b. Laser Ablation

Laser ablation (also known as pulsed laser deposition, or PLD) is the use of a high-intensity pulsed laser beam to irradiate a target material, producing ejection of micron-sized particulates during the ablation process. The expelled particulates were caused by the high energy of the pulse laser and can significantly affect the optical properties of deposited films [27]. When the pulsed laser beam is absorbed by the target, energy is converted into thermal, chemical, and mechanical energy and this is followed by evaporation, ablation, plasma generation and sometimes even exfoliation [28].

A simplified diagram of a typical PLD process is shown in FigureI.5 illustrating a vacuum chamber equipped with a window, a substrate holder and a target material. The vacuum environment is crucial to minimize interactions with impurity gas molecules. The Substrate holder secures the substrate in place and cab be modified to apply heat or an electrical current during the deposition. The target serves as the source material to be deposited on the substrate. When the pulsed laser beam strikes the target, it generated an ablation plume directed toward the substrate where the material condenses to form a thin film [29].

PLD targets are typically developed by thoroughly mixing small quantities of finely ground powders of the desired material into a liquid and then compressing them into pellets, and subjecting them to a controlled heat treatment (sintering) which is the process of heating the material to a temperature below its melting point in order to attach the particles together to form a solid, dense structure [30].

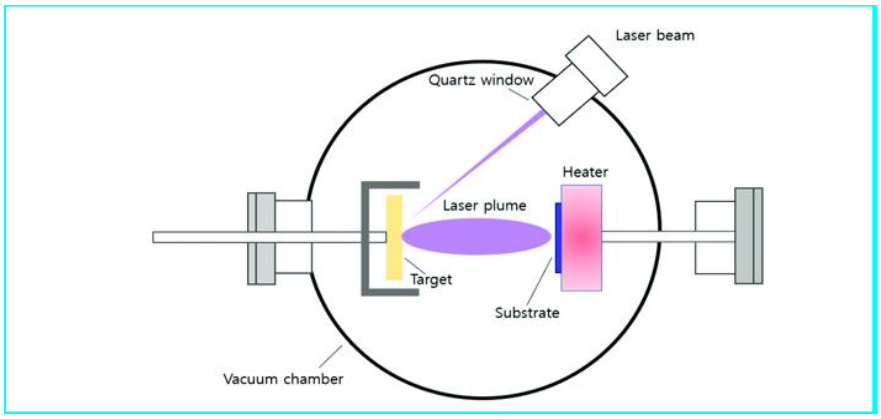

Figure I.5: Schematic of the PLD process [31].

I.4.1.1.c. Sputtering Technique

Sputter deposition is a widely used physical vapor deposition (PVD) technique for growing thin films due to its cost-effectiveness, simplicity, ability to cover large areas, and low-temperature requirements [32].

This process involves ejecting material from a cathode and depositing it onto a substrate through ion bombardment. The sputtering system typically consists of a vacuum chamber housing a metallic anode and cathode. When a voltage of several Kev is applied under a pressure above 0.01 mbar, a glow discharge occurs, releasing ions that strike the cathode and dislodge target atoms with high kinetic energy.

For optimal momentum transfer, the bombarding ions should have a mass similar to the target material. These sputtered atoms travel linearly and accumulate on the substrate, forming a dense, uniform thin film [33]. A schematic representation of the sputtering process is illustrated in Figure I.6, which highlights the fundamental stages of ion bombardment and thin-film growth.

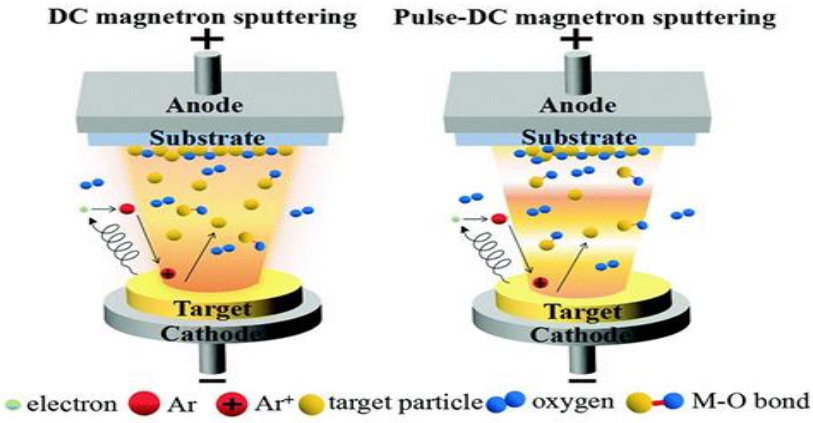

Figure I.6: Sputtering system diagram [34]

I.4.2 Chemical Deposition Methods

I.4.2.1 Chemical Vapor Deposition (CVD)

Chemical Vapor Deposition is a chemical process used to the deposit of thin film by introducing gaseous precursor onto a heated substrate. The process involves adding volatile compounds along with a carrier gas to a reaction chamber, where controlled chemical reactions take place forming solid films that are highly pure and structurally uniform. CVD can be divided into thermal CVD, plasma-Enhanced CVD (PECVD) and atomic layer deposition (ALD), which each provides advantages in terms of temperature requirements, film deposition rate and

film quality. CVD is used worldwide for several advanced applications including the fabrication of semiconductor devices, optical coatings, and functional material synthesis.

I.4.2.1.a. Atomic Layer Deposition (ALD)

Atomic Layer Deposition (ALD) is a vapor-phase technique based on sequential self-limiting surface reactions. In ALD, precursors are alternately introduced into the reaction chamber under controlled conditions (e.g., temperature, pressure and precursor chemistry), ensuring complete surface saturation at each step. This mechanism enables the deposition of highly uniform and conformal thin films even on complex 3D structures, making ALD ideal for applications requiring atomic -scale precision. [35]

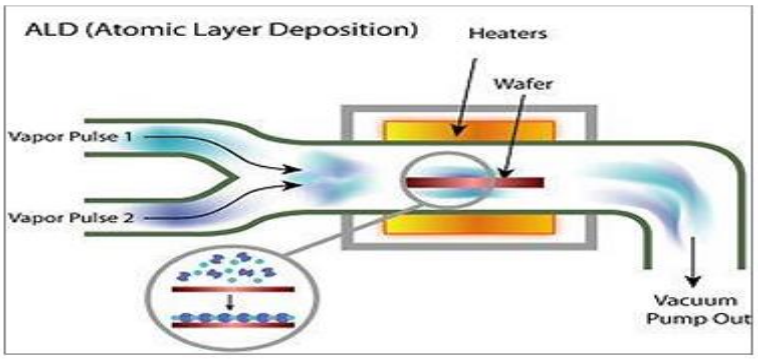

Figure I.7: Principle of Atomic Layer Deposition (ALD) [36].

I.4.2.1.b. Thermal CVD

The thermal process (or Thermal CVD) is the most common sub-technique of the Chemical Vapor Deposition (CVD) process. Substrate heating is applied in this process for supplying the energy needed for driving the chemical reaction and enhancing atom diffusion. There are a number of ways for performing this heating:

- ✓ **Joule heating**: Generated by flowing an electric current through the substrate, utilizing its resistive property.
- ✓ **Thermal radiation heating:** Uses a heating rod (such as tungsten) to raise the chamber temperature, ensuring better coating uniformity by enhancing atom mobility.
- ✓ **High-frequency induction heating:** requires the substrate tp possess both electrical and thermal conductivity [37].

This process enables the formation of uniform thin film by controlling reaction kinetics and material diffusion.

I.4.2.1.c. Plasma-Enhanced CVD (PECVD)

Plasma-Enhanced Chemical Vapor Deposition (PECVD) is widely used technique for depositing thin films at low temperatures on a various substrate. This method involves applying an electric field to a chamber containing a reactive gas which generates reactive species such as (ions, electrons, radicals, etc.) through the excitation or dissociation of the gas molecules via electron collisions.

At the substrate surface, these reactive species undergo chemical reactions, leading to the formation of a thin film. Additionally, ion bombardment can modify the substrate surface, enhance the adsorption of certain species or promote the desorption of others.

PECVD is versatile and can be used for thin-film deposition as well as etching processes [38].

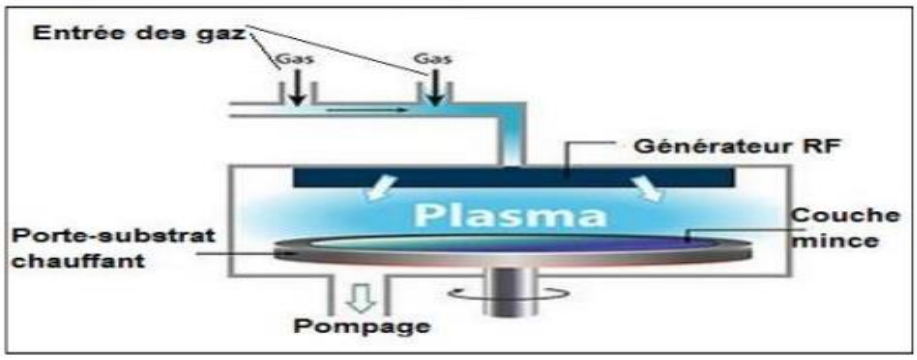

Figure I.8: Experimental Setup of PECVD [39].

I.4.2.2 Sol-Gel Method

The Sol-gel process is a widely used synthesis method in which molecular precursors in a liquid solution (sol) undergo polymerization, forming an oxide network (gel). This method involves a drying stage followed by thermal treatments to remove of organic components, resulting in an inorganic oxide material. The sol-gel technique is particularly useful in the making of materials of homogenous materials, including powders and thin films, with excellent optical properties [40]. There are two main techniques for depositing sol-gel films:

I.4.2.2.a. Spin-Coating (Centrifugation)

This technique involves depositing the sol or gel onto rapidly a rotating substrate where the centrifugal force ensures uniform spreading of the liquid, while excess material is expelled.

The final thickness of the coating will be determined by the centrifugal speed, viscosity of the solution and deposition time. This method is widely used for thin film production due its uniformity in. A schematic of the spin-coating process is shown in Figure I.9 [42].

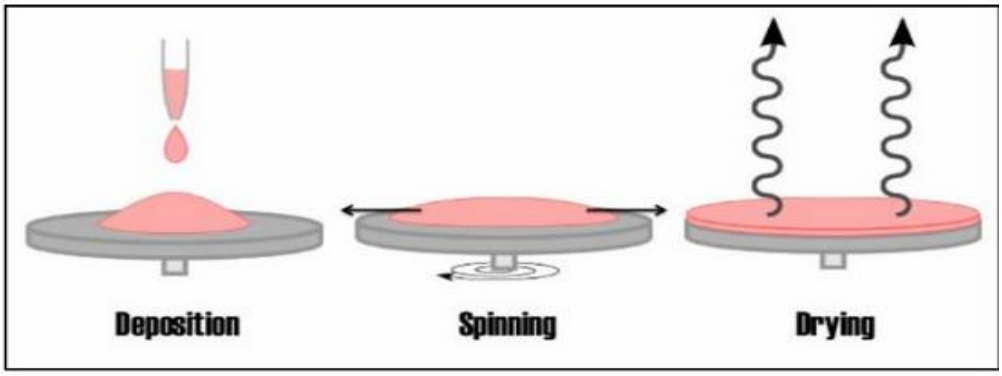

Figure I.9: schematic illustration of the spin coating process [41].

I.4.2.2.b. Dip-Coating

This technique involves immersing a substrate into a solution containing hydrolysable metal components, then withdrawing it at controlled speed, temperature, and atmosphere (Figure I.10) [43]. Hydrolysis and condensation reactions occur during this process, forming uniform coating. The Film thickness depends on the withdrawal speed, solid content and solution viscosity. High-temperature treatments improve film properties but must be carefully controlled to avoid cracking [43]. While dip-coating is not as commonly used, it is suitable for large-area applications and allows precise control over film thickness with a high uniformity [44].

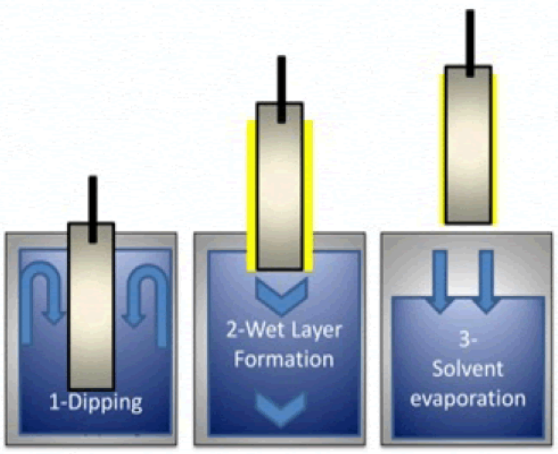

Figure I.10: A graphical illustration of the dip coating technique [45].

This process is typically carried out either at room temperature or at at temperatures not exceeding 100<C, depending on the solvent used. Figure I.11 shows a typical sol-gel process applicable for both thin films and powders [46].

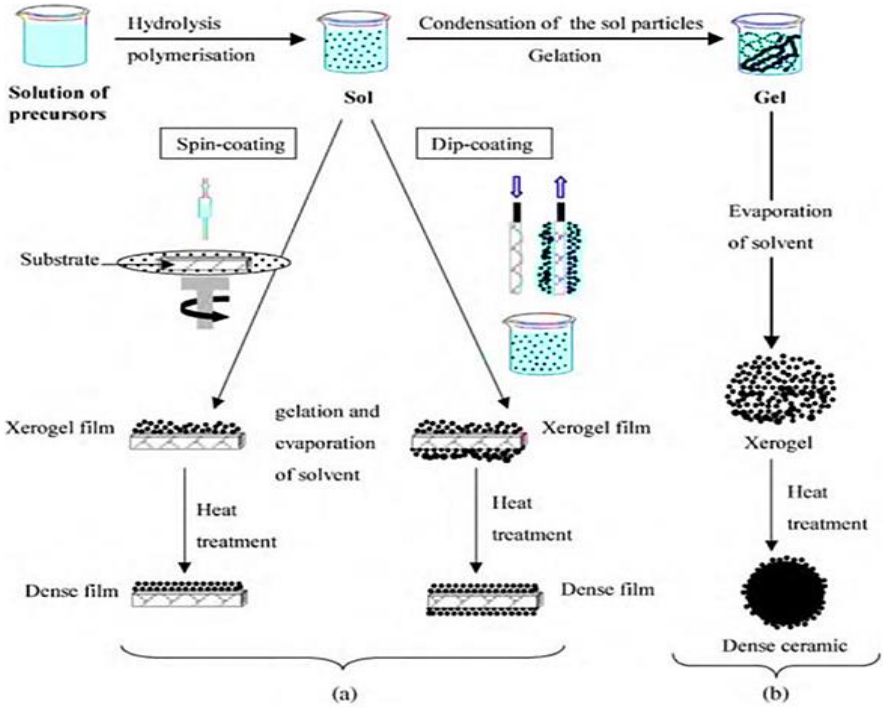

Figure I.11: Overview showing two synthesis examples by the sol–gel method; (a) films from a colloidal sol; (b) powder from a colloidal sol transformed into a gel [46].

The three main steps of the sol-gel process are:

1. Preparation of the starting solution, which includes a solvent, a precursor and the required additives.

2. Deposition of the prepared solution onto substrates using various techniques, such as dip-coating (M. Ohyyama, 1997) [47] and spin-coating (M.N. Kamalasanan, 1996) [48].

3. Pre-heating of the samples at an elevated temperature to evaporate the solvent, leaving behind a xerogel film or matrix.

The process of applying the solution to the substrate and drying it is repeated multiple times until the desired film thickness is achieved. The sample is then post-heated (annealed) to form the final crystalline structure and eliminate any unwanted organic material.

For powder production, the gels are typically dried temperature. In, the sol-gel process, it is difficult to distinguish between primary particles (small grains or crystallites) and secondary particles (agglomerates of primary particles) because grain growth and

agglomeration occur simultaneously [49]. Figure I.12 illustrates the Formation of primary particles (~2 nm in diameter) that aggregate into secondary particles (~6 nm).

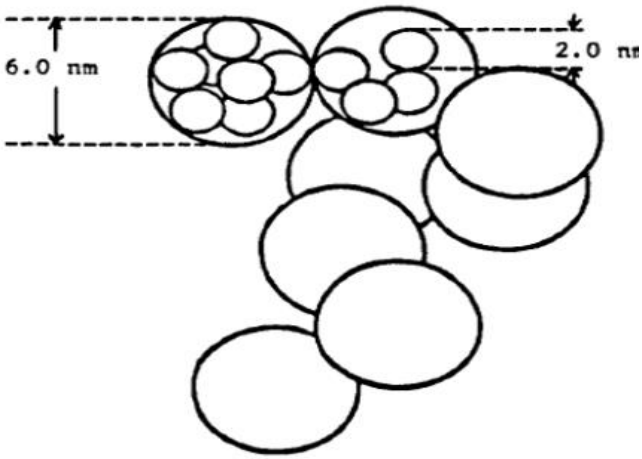

Figure I.12: Schematic representation of primary and secondary particles in alkoxide gel [50]

I.4.2.3 Spray Pyrolysis

The spray pyrolysis deposition method is being used for thin/thick film development, ceramic coatings, and powders. The main advantages of this technique are low cost and easy handling while giving good results. Spray pyrolysis has been used for several decades now in the glass industry [51] and in the production of solar cells [52].

Essentially, the method relies on the vaporization and spraying of a solution containing various reactive compounds onto a heated substrate, using an atomizer. The substrate temperature promotes chemical reactions amongst the compounds which then leads to the formation of the desired material [53].

A detailed discussion of the mechanisms and technical aspects of this method will be discussed in another chapter.

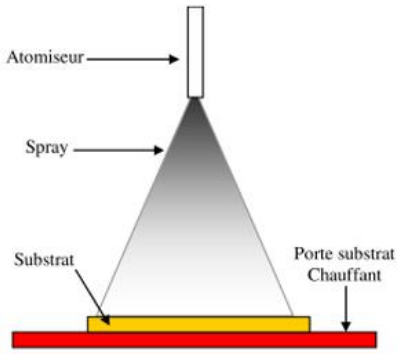

Figure I.13: Schematic Diagram of the Spray Pyrolysis Deposition Principle.

I.5.Conclusion

This chapter has provided a comprehensive overview of the fundamental principles of photovoltaic technology and thin-film deposition techniques relevant to solar energy. It addressed the core concepts of photovoltaic effect, the structure and operational mechanism of solar cells, and the pivotal role of thin films in enhancing the efficiency and performance of photovoltaic devices. Furthermore, a detailed examination of both physical and chemical deposition methods was presented, outlining the underlying mechanisms advantages, and limitations associated with each technique.

References

[1] S. Benghabrit, "Propriétés générales des semi-conducteurs", Thèse de Doctorat, (2006).

[2] K. Emery, J. Burdick, Y. Caiyem, D. Dunlavy, H. Field, B. Kroposki, T. Moriarty, L. Ottoson, S. Rummel, T. Strand, M.W. Wanlass, "Temperature dependence of photovoltaic cells, modules and systems", Proceedings of the 25th IEEE Photovoltaic Specialists Conference, 13–17 May (1996), pp. 1275–1278.

[3] A. Cid Pastor, "Conception et réalisation de modules photovoltaïques électroniques", Thèse de Doctorat, Institut National des Sciences Appliquées de Toulouse, (2006).

[4] K. Helali, "Modélisation d'une cellule photovoltaïque", Mémoire de Magister, Université Mouloud Mammeri de Tizi-Ouzou, (2012).

[5] A.T. Singo, "Système d'alimentation photovoltaïque avec stockage hybride pour l'habitat énergétiquement autonome", Thèse de Doctorat, Université Henri Poincaré, Nancy-I, (2010).

[6] O. Nichiporuk, "Simulation, fabrication et analyse de cellules photovoltaïques à contacts arrière inter-digités", Thèse de Doctorat, Institut National des Sciences Appliquées de Lyon, (2005).

[7] S. Guitouni, "Corrélation entre les propriétés thermo physiques des gouttelettes et les propriétés des couches minces déposées par le procédé spray", Mémoire de Magister, Université de Constantine, (2010).

[8] T. Ait Ahcene, "Élaboration et caractérisation des couches minces de sulfure de zinc avec diffusion de l'argent et du manganèse", Mémoire de Magister, Université de Constantine, (1992).

[9] T. Dauzhenka, "Couches minces d'oxyde d'étain : la localisation faible et les effets de l'interaction", Thèse de Doctorat, Université de Toulouse, (2011).

[10] A. Lachgueur, "Étude des couches minces de ZnO dopées", Mémoire, Université de Tlemcen, Juin (2015).

[11] C. Bilzer, "Susceptibilité micro-ondes de couches minces ferromagnétiques : métrologie et analyse de la dynamique de l'aimantation", Thèse, Université Paris 11, (2007).

[12] M. Hehn, "Magnétisme et transport polarisé en spin : de la couche mince aux dispositifs à électronique de spin", Thèse, Université Henri Poincaré-Nancy I, (2004).

[13] R. Benrabbah, "Développement de procédés plasma pour l'élaboration et la caractérisation du silicium photovoltaïque : dépôt de couches minces épitaxiées de silicium par PECVD, mesure de la pureté du silicium à l'état solide (20 °C) et liquide (1414 °C) par LIBS", Thèse, Université Pierre et Marie Curie-Paris VI, (2015).

[14] K.E. Drexler, "Nano systems: Molecular Machinery, Manufacturing, and Computation", John Wiley & Sons, Inc., (1992).

[15] P. Roca i Cabarrocas, "Thèse de Doctorat", Université Paris VII, (1988).
[16] S. Guitouni, "Corrélation entre les propriétés thermo physiques des gouttelettes et les propriétés des couches minces déposées par le procédé spray", Mémoire de Magister, Université de Constantine, (2010).

[17] Y. Benkhetta, "L'effet du débit de la solution sur les propriétés des couches minces d'oxyde de zinc (ZnO) déposées par spray ultrasonique", Mémoire de Magister, Université Mohamed Khider Biskra, Algérie, (2013).

[18] R. Khaoua, A. Zatout, "Élaboration des couches minces ZnS par la méthode spin coating pour application en photocatalyse des polluants organiques", Mémoire de Master, Université Kasdi Merbah Ouargla, Faculté des Sciences Appliquées, Département de Génie des Procédés, Option : Génie de l'environnement, (2020).

[19] K.L. Chopra, S. Major, D.K. Panday, "Thin Solid Films", (1983), pp. 102–105.

[20] O. Darenfad, Mémoire de Magister, Université Mentouri Constantine, (2017).

[21] K. Medjnoun, "Étude et réalisation de semi-conducteurs transparents ZnO dopé vanadium et oxyde de vanadium en couches minces pour des applications photovoltaïques", Thèse de Doctorat, Université Mouloud Mammeri de Tizi-Ouzou, (2015).

[22] A. Allag, Mémoire de Master 2, Université Mohamed Khider Biskra, (2013).

[23] L.T. Sollac (Groupe Usinor), "Les traitements de surface sous vide", La Revue de Métallurgie - CIT, avril (2001).

[24] M. Mostafa, "Dépôt et caractérisation de couches minces de ZnO par spray pyrolysis", Mémoire de Magister, Université de Biskra, (2005).

[25] S. Lamri, "Élaboration et caractérisation des couches minces de ZnO dopées par l'indium", Mémoire de Master, Université Mohamed Khider Biskra, (2012).

[26] R. Prabu, S. Ramesh, M. Savitha, M. Balachandar, "Proceedings of the International Conference on Sustainable Manufacturing", vol. 427, (2013).

[27] D.B. Chrisey, G.K. Hubler, Pulsed Laser Deposition of Thin Films, John Wiley & Sons, (1994).

[28] R.J. Martín-Palma, A. Lakhtakia, Vapor-Deposition Techniques, Chapitre 15, Elsevier Inc., (2013).

[29] R. Eason, Pulsed Laser Deposition of Thin Films, John Wiley & Sons, New Jersey, (2007).

[30] M.M. Almotari, "Fabrication and Characterisation of Zinc Oxide Thin Films Singly Doped with Trace Amounts of Rare Earth Materials", PhD Thesis, University of Canterbury, (2013).

[31] C. Song, H.J. Kwon, "Ferroelectrics Based on HfO_2 Film", Electronics, vol. 10, (2021), p. 2759.

[32] M. Ohring, Materials Science of Thin Films: Deposition and Structure, Academic Press, San Diego, (2002).

[33] D. L. Smith, Thin-Film Deposition: Principles and Practice, McGraw-Hill, New York, (1995), p. 187–200.

[34] H. Angusmacleod, "Recent developments in deposition techniques for optical thin films and coatings", in A. Piegari, F. Flory (eds), Optical Thin Films and Coatings from Materials to Applications, Woodhead Publishing, Oxford, (2013), pp. 3–25.

[35] SIMAP Grenoble-INP, "Dépôts de couches atomiques (ALD)", [en ligne], disponible sur : https://simap.grenoble-inp.fr/, consulté le 31 mai (2025).

[36] Pinterest, "SMR: Atomic Layer Deposition Market Dynamics, Forecast, Analysis and Supply Demand 2014-2020", [en ligne], disponible sur : https://br.pinterest.com/, consulté le 31 mai (2025).

[37] Citra Limousin, "Les Dépôts Par CVD Laser Thermique OMCVD et PECVD", [en ligne], disponible sur : https://www.citra-limousin.com/traitements, consulté le 31 mai (2025).

[38] M. Kihel, "Caractérisation de films minces déposés par plasma PECVD à partir de vapeurs de TMS", mémoire de magister, Université Mentouri de Constantine, (2006).

[39] K. Djebbar, K. Zerroug, "Elaboration par bain chimique et étude des couches minces de sulfure cadmium (CdS) et sulfure de cuivre (CuS)", Université Larbi Ben M'hidi Oum El Bouaghi, (2017).

[40] I. Wuled Lengooro, Y. Chan Kang, T. Komiya, K. Okuyama, N. Tohge, "Journal of Applied Physics", (1998), pp. 288–290.

[41] S.L. Hellstrom, "Basic models of spin coating", (cours pour Physics 210, Stanford University), (2007).

[42] J. Livage, M. Henry, C. Sanchez, "Progress in Solid State Chemistry", vol. 18, (1988), pp. 259–341.

[43] K. Bennaceur, "Élaboration et caractérisation des couches minces de SnO_2 : In déposées par la technique de pyrolyse par pulvérisation ultrasonique", Thèse de Doctorat, Université Mohamed Khider de Biskra, (2020).

[44] I. Kentari, N. Tatsuo, "Japanese Journal of Applied Physics", vol. 50, no. 5, (1985), p. L245.

[45] S.B. Khan, H. Wu, C. Pan, Z. Zhang, "A mini review: Antireflective coatings processing techniques, applications, and future perspective", Journal of Material Sciences & Engineering, vol. 6, no. 4, (2017), p. 192.

[46] A.C. Pierre, "Introduction to Sol-Gel Processing", Springer, New York, (1998).

[47] J. Livage, D.G., "Sol-gel electrochromic coatings and devices: a review", Solar Energy and Materials and Solar Cells, vol. 68, (2001), pp. 365–381.

[48] L. Znaidi, "Sol–gel-deposited ZnO thin films: A review", Materials Science and Engineering: B, vol. 174, no. 1–3, (2010), pp. 18–30.

[49] D.L. Zayat, "The Sol-gel Handbook part one", Wiley-VCH, Weinheim, (2015).

[50] S. Chang, R. Doong, "ZrO_2 thin films with controllable morphology and thickness by spin coated sol–gel method", Thin Solid Films, vol. 489, (2005), pp. 17–22.

[51] J.M. Mochel, "US Patent 2,564,707", (1951).

[52] J.E. Hill, R.R. Chamberlin, "US Patent 3,148,084", (1964).

[53] K. Kamli,"Étude et élaboration des composés binaires et ternaires destinés à des applications photovoltaïques", thèse de doctorat, Université Badji Mokhtar-Annaba, (2017).

Chapter II:

Characterization and Preparation of Tin Sulfide (SnS) Thin Films

II.1. Introduction

This chapter provides on overview of thin sulfide (SnS) thin films, focusing on their material properties, preparation methods, and characterization techniques. SnS is a promising material for photovoltaic applications due to the favorable bandgap and high absorption efficiency. The chapter covers the selection of SnS as a material, the phase diagram of the Sn-S system, and its optical, electrical, and growth characteristics; relevant key experimental techniques for the analysis of SnS thin film such as ultrasonic spray pyrolysis, X-ray diffraction, and UV-visible spectrophotometry are added. Preparation of SnS: Mg thin films through ultrasonic spray pyrolysis is presented, explaining the main steps in substrate preparation, formulation of precursor solutions and deposition.

II.2. Tin Sulfide (SnS)

Tin sulfide (SnS) was first investigated in the early 20th century, with the German mineralogist Herzenberg reporting it for the first time in 1932 [1]. Since then, many investigations have examined its structural, optical, and electronic properties for use in optoelectronic applications [2].

SnS has an orthorhombic crystalline structure that has stability and good electronic properties; thus, the material is potentially suitable for photovoltaic and optoelectronic devices [2]. Moreover, it possesses good thermal stability, thus improving its viability for thin film technologies [3]. Jiang and Ozin [4] mentioned that SnS can be doped with a variety of metallic and non-metallic elements to improve its physical and chemical properties, making it a suitable candidate for developing advanced functional materials.

II.2.1 Choice of SnS Material

Tin(ii) monosulfide (SnS) stands out as one of the best optoelectronic materials having properties that can make it a suitable candidate for an absorber in solar cells. The selection of SnS in this study is based on the following key characteristics: [5]

• High chemical and thermal stability during operating conditions

• An optical bandgap of about 1.3 eV, closely matching the ideal value for maximum conversion efficiency of solar energy.

• High optical absorption coefficient (> 10^5 cm^{-1}), which means that an extremely thin layer of just a few microns can absorb all photons having energies greater than the bandgap energy.

• Dual p- and n-type conductivity, depending on the tin concentration, allowing for the fabrication of homojunctions.

Given these advantages, SnS is chosen as the primary absorber in this work.

II.2.2. Phase Diagram of the Sn-S System

Albers et al. presented a comprehensive study on the phase equilibria involving the solid, liquid, and gaseous states of the Sn–S system, particularly focusing on the formation of tin monosulfide (SnS). Their work established the phase diagram of the system, illustrating the stability and transformation of different phases composed of tin (Sn) and sulfur (S). [6]

This phase diagram is of great importance because it provides insight into the thermodynamic conditions under which various tin sulfide compounds, such as SnS, SnS_2, and Sn_2S_3 are formed. Specifically, it helps determine the formation domains of these compounds based on the sulfur-to-tin (S-Sn) atomic ratio and the temperature. Understanding these conditions is essential for optimizing the synthesis process and ensuring the desired phase is obtained in thin film or bulk material applications.

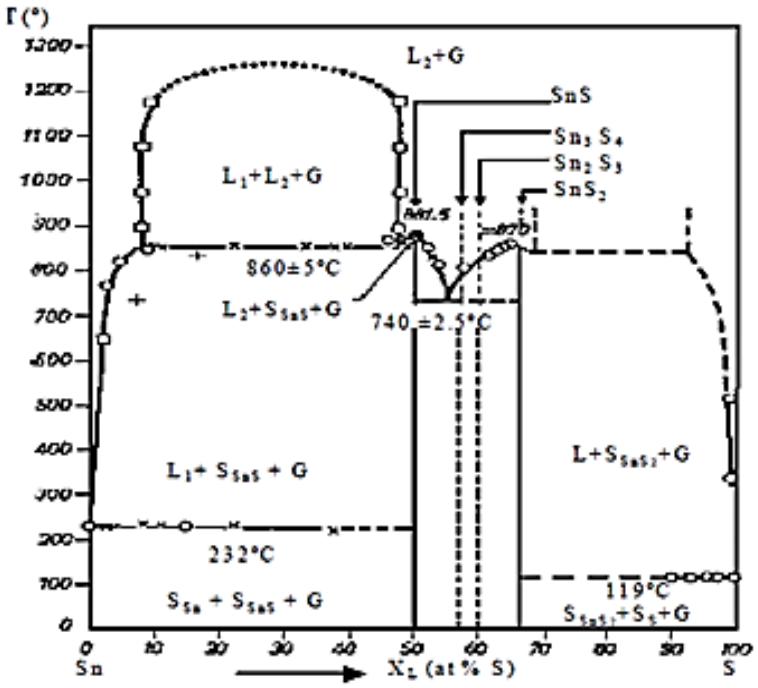

Figure II.1. Phase of the SnS system

II.3. Physical properties of SnS

II.3.1 Macroscopic Appearance of Tin Sulfide

Several studies have shown that the color of tin sulfide (SnS) thin films is primarily influenced by their crystalline phase and deposition temperature [7]. According to Lee A. Burton et al., three different phases exist in the Sn-S system; namely, (i) SnS: dark gray films; (ii) Sn_2S_3: black needle-like structures; and (iii) SnS_2: yellow flakes (see Figure II.2). [8].

Variations in color are attributed to differences in crystal structures and chemical composition, which modify the absorption and reflection properties. The deposition conditions play a critical role in determining the dominance phase, thereby directly influencing the optical and electronic properties of the resulting material.

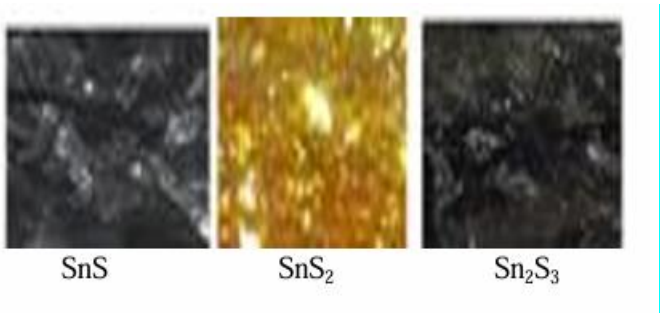

Figure II.2: Macroscopic appearance of tin sulfide [8].

II.3.2 Growth Mechanisms and Kinetics

The deposition parameters that influence the thickness of tin sulfide (SnS) thin films include temperature, deposition time, solution concentration, and flow rate. Figure II.3 shows the effect of deposition temperature on the thickness of SnS films synthesized using the Chemical Bath Deposition (CBD) method.

The growth of these films is gradual, as initial particles settle onto the substrate and progressively build up the thickness until a stable structure is achieved. However, Longer deposition times may sometimes lead material rearrangement, while surface chemical interactions can cause a slight reduction in thickness [9].

By carefully adjusting the deposition conditions, it is possible to control the film's thickness and optimize its physical properties for various applications, especially in solar cells.

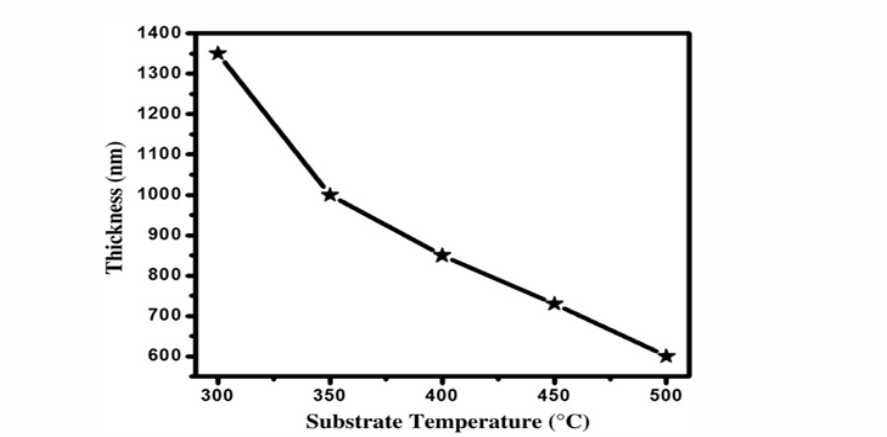

Figure II.3: Variation of film thickness with substrate temperature [9].

II.3.3 Crystal Structure

Tin(II) sulfide (SnS) exhibits multiple crystal structures due to the ability of thin (Sn) to adopt two oxidation states ,Sn(II) and Sn(IV).In its most stable form at low temperatures ,SnS crystallizes into an orthorhombic Pnma structure, characterized by a layered arrangement of two-dimensional sheets (Figure II.4.a) [10].The Sn^{2+} ion coordinates with S^{2-} ions, while the lone electron pair of Sn occupies the remaining position in a distorted tetrahedral geometry.

In addition to the orthorhombic Pnma phase, SnS can also form other polymorphs, including the rock salt (Fm-3m), the high-temperature orthorhombic Cmcm, and the zincblende (F-43m) structures (Figure II.4. b–d) [10].

Tin disulfide (SnS_2), which has been synthesized for over 200 years, crystallizes in a hexagonal P-3m1 structure, where Sn (IV) ions coordinate octahedrally to sulfur in a layered configuration similar to rutile SnO_2 (Figure II.4. e) [11,12]. Weak van der Waals interactions hold the SnS_2 trilayers together.

Tin sesquisulfide (Sn_2S_3) adopts an orthorhombic Pnma structure, containing both Sn (II) and Sn (IV) oxidation states. Unlike SnS, Sn_2S_3 consists of one-dimensional chains, where Sn (IV) ions occupy central positions with octahedral coordination, while Sn (II) ions adopt trigonal-pyramidal arrangements at the chain ends (Figure II.4. f) [10,12]

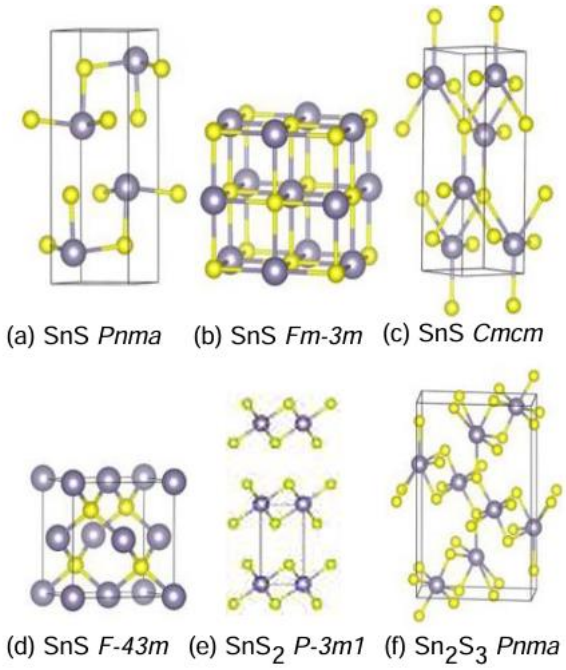

Figure II.4. (a-d) crystal structure of various SnS polymorphs, (e) SnS_2 and (f) Sn_2S_3 (Sn and S in grey and yellow color, respectively) [10]

II.3.4 Optical Properties of SnS

Tin sulfide (SnS) has attracted considerable attention in recent years due to its promising optical properties, which are crucial for its application as an absorber layer in thin-film solar cells, one of the main advantages of SnS is its direct optical band gap of approximately 1.30 eV, which is close to the optimal value for solar energy conversion (1.50 eV) [13]. This allows for efficient absorption of incident solar radiation.

The refractive index of SnS is around 3.5, and the films generally demonstrate low transmittance in the visible range (400-800 nm), which is beneficial for photovoltaic applications. The absence of interference fringes in the transmittance spectra (Figure II.5) suggests that the surface of the SnS films is relatively rough [14].

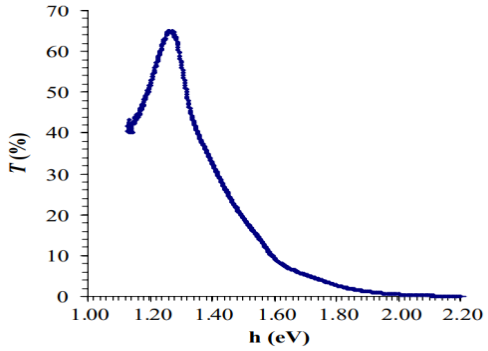

Figure II.5: Dependence of the transmittance versus the photon energy [15].

Table II.1: The optical band gap of SnS material by different techniques

Technique	Cathodic electrodeposition	Spray	CBD	Thermal evaporation	Pulsed electrodeposition	Co-evaporation
Eg(ev)	**1.15(19)**	**1.30-1.40 (17)**	**1.75-1.15(15)**	**2.15-2.30 (18)**	**1.46-2 (20)**	**1.75 (16)**

Table II.1 summarizes the optical band gap (Eg) values of SnS thin films obtained through various deposition techniques, such as cathodic electrodeposition, spray pyrolysis, chemical bath deposition (CBD), thermal evaporation, co-evaporation, and pulsed electrodeposition. The reported Eg values range from 1.15 eV to 2.30 eV, depending on the technique and deposition parameters [15, 16, 17, 18, 19, 20].

II.3.5 Electrical Properties of SnS

Numerous studies have investigated the electrical behavior of tin sulfide with the goal of optimizing its performance for electronic and photovoltaic applications.

The electrical resistivity SnS thin films with an orthorhombic structure and without annealing typically falls within the range of 10^5 and 10^6 Ω·cm in the dark. Similarly, SnS films with a zinc blende structure, under the same conditions have been reported to exhibit a resistivity of approximately 1.7×10^7 Ω·cm [21].

It is widely accepted that such high resistivity is not favorable for solar cell applications. However, various fabrication methods have been developed to produce SnS films with signification reduced resistivity. For example, as recently reported by Gao Chao, Honglie Shen and Sun Lei, thin film produced via the chemical bath deposition have achieved dark resistivity values as low as 10^2-10^5Ω·cm, which is highly promising for the development of future low-cost solar cells using SnS as the absorber layer.

In addition, SnS exhibits dual conduction types, namely p-type and n-type conductivity, which enhances its versatility for semiconductor device applications [22].

Table *II.2: summarizes the electrical properties of SnS films prepared using various deposition techniques. [22]*

Growth technique	**Type**	**Carrier density (cm-3)**	**Mobility (cm2V-1S-1)**	**Resistivity (Ω·cm)**	**Activation energy (ev)**	**Ref**
CBD	P	-	8.99×10^5	2.53×10^5	0.527	[23]
Electron-beam evaporation	-	10^{17}	1.2	51	-	[24]
Spray	P	1.6×10^{15}	130	37-25	0.46	[25]

II.4. Experimental Techniques

The experimental device used in this study was designed and assembled at the Semiconductor Laboratory of the University of Annaba. It is built from simple components, which have been modified to allow for the deposition of relatively homogeneous thin films of the selected material. The basic principle and structure of the ultrasonic spray deposition system we developed are shown in Figure II.6.

Figure II.6: Experimental ultrasonic spray setup

This system was adapted specifically to ensure good control over deposition parameters such as substrate temperature, droplet size and nozzle-to-substrate distance, in order to improve the uniformity and quality of the resulting thin films.

II.4.1 Ultrasonic Spray Pyrolysis (USP)

II.4.1.1 Experimental Setup

The Ultrasonic Spray Pyrolysis (USP) technique is an efficient and cost-effective method preparing thin-films, particularly for materials like Tin Sulfide (SnS) and their various doped forms such as SnS: Mg. The setup for the ultrasonic spray pyrolysis technique involves several components working together to convert the precursor solution into a fine mist, which is then deposited on a heated substrate to form the thin film. The experimental setup for the preparation of SnS: Mg thin films will be described in this section.

II.4.1.2. Working Principle of Ultrasonic Spray Pyrolysis

The working Principle of ultrasonic spray pyrolysis is similar to conventional spray pyrolysis, with the key difference being the use of ultrasonic energy to atomize the precursor solution into a fine mist. In ultrasonic spray pyrolysis, an ultrasonic nebulized is employed to

convert the precursor solution into a fine mist that is directed toward the heated substrate. The process begins with the generation of high-frequency acoustic waves (typically in the range of 20-40KHz) causing the liquid to vibrate and form fine droplets.

The droplets size typically ranges from 20 to 40 micrometers and these droplets are directed toward the heated substrate ,where they undergo pyrolysis at the desire temperature .The ultrasonic waves create surface instability in the liquid, leading to the formation of droplets through the interaction of the wave crests .When these droplets reach the heated substrate (in this study, the substrate is maintained at 350 °C) ,volatile components of the solution are evaporated, leaving behind the desired compounds that deposit onto the substrate creating the thin film.

This technique offers precise control over droplet size and uniformity of the deposited thin films. As a result, High-quality, homogeneous thin films with uniform thickness are obtained, making this method ideal for large -area application such as solar cells. In our experiment, the ultrasonic nebulizer was operated at the frequency of 40 kHz for 30 minutes with a constant distance of 4.5 cm between the nozzle and the substrate.

The substrate was kept at a constant temperature of 350°C during the deposition process ensuring proper crystallization of the SnS: Mg films and resulting in optimal thin film quality. The schematic diagram of deposition system we developed is shown in Figure II.7.

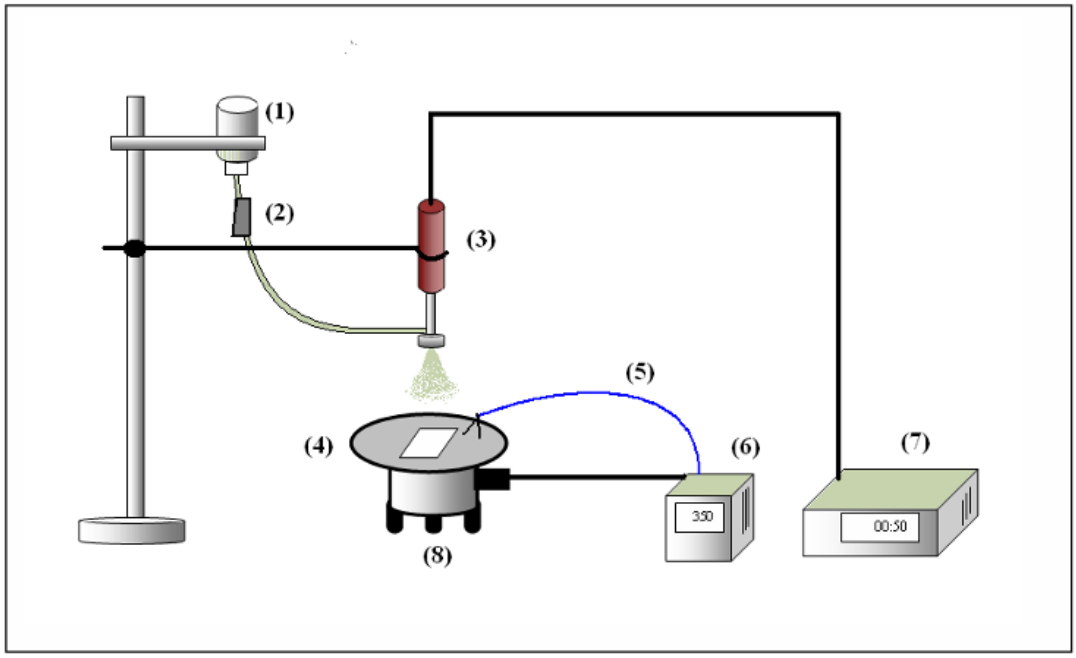

Figure II:7 Schematic Diagram of the Ultrasonic Spray Pyrolysis System [26]

1. Solution flask
2. Flow controller
3. Atomizer
4. Substrate holder
5. Thermocouple
6. Temperature regulator
7. Ultrasonic generator
8. Resistive heater

II.4.2. X-ray Diffraction (XRD)

X-ray diffraction is generally used for the structural characterization of materials [27]. It identifies the crystalline phases present in the sample and provides an evaluation of their crystallinity. It also offers information about the crystallographic growth directions of thin films [28].

II.4.2.1Principle

When a monochromatic X-ray beam is directed at a polycrystalline material, it is partially reflected by the atomic planes of some crystals. The interference of the scattered rays may be constructive or destructive, depending on the spatial direction. As a result, strong or weak X-ray signals are observed; these variations correspond to the directions forming the X-ray diffraction phenomenon [29]. A detector captures the diffracted X-ray beam from the sample and records their intensity as a function of the diffraction angle 2θ. When Bragg's law is satisfied, a diffraction peak corresponding to the specific family of planes appears in the diffractogram [30]

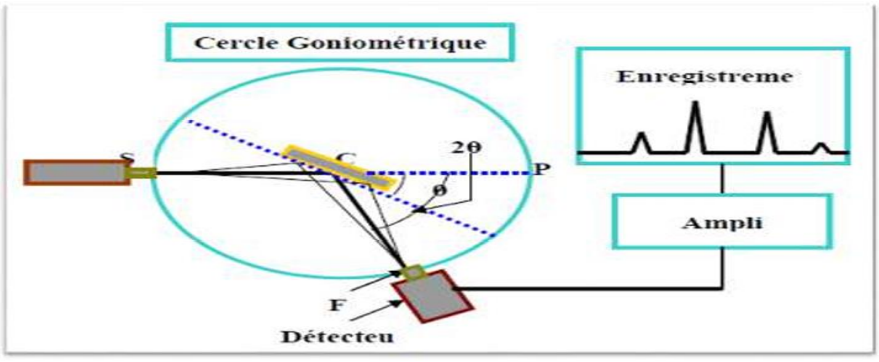

Figure II.8. Principle of X-ray diffraction.

II.4.2.2. Bragg's Law

The direction where constructive interference occurs, called "diffraction peaks ", are determined by Bragg's law, which is expressed as:

$$2d_{hkl}\sin(\theta_{hkl}) = n\lambda \quad \text{(II.1)}$$

Where:

- d_{hkl}: is the interplanar spacing between crystal planes.
- λ: is the wavelength of the X-rays.
- n: is the diffraction order.
- θ_{hkl}: the angle between the incident beam and the diffracting planes with Miller indices [31].

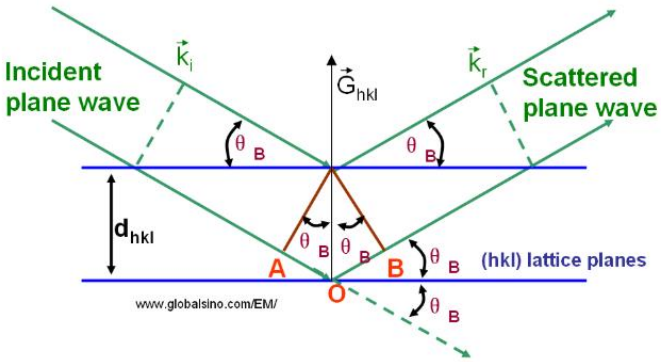

Figure II.9. Bragg's Law reflection

II.4.2.3. Determination of Crystallite Size

From the diffraction spectra, the crystallite size of each deposited phase can be estimated using the Scherrer formula, given by the following relation [32]:

$$\mathbf{D}=\frac{(0.9.\lambda)}{\beta.Cos\theta} \quad \text{(II.2)}$$

Where:

- D: is the average crystallite size.
- β: is the full width at half maximum (FWHM) in radians of the diffraction peak at 2θ.
- θ: is the diffraction angle in degrees.

- λ: is the wavelength of the X-ray beam (Å) [29]

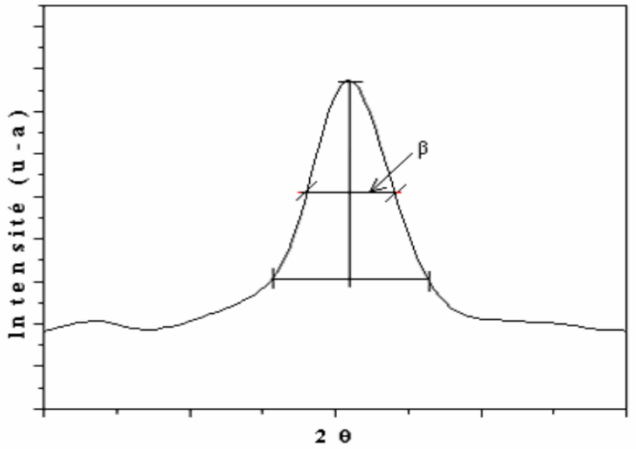

Figure II.10. Illustration Showing the Definition of β from the X-ray Diffraction Curve.

II.4.2.4 Experimental Setup

In this study, the Crystalline structure of the Mg-doped SnS thin films was characterized using an X-ray diffractometer (Malvern PANalytical® Empyrean Series) equipped with a using a Cu-Kα radiation source of wavelength 1.5418 Å. The diffraction patterns were recorded over a 2θ between range from 10°to 80°which allowed for comprehensive analysis of the analysis of crystallographic structure and phase composition of the synthesized thin films [33].

Figure II.11: X-ray Diffractometer (Malvern PANalytical® Empyrean Series).

II.4.3 UV–Visible Spectrophotometry

UV-visible spectrophotometry is widely employed to analyze the optical properties of thin film materials. It provides valuable information about the optical absorption edge, absorption coefficient, optical band gap, Urbach energy, and refractive index. In certain cases, this technique can also be used estimate the film thickness.

II.4.3.1. Principle

The working principle of a UV-visible spectrophotometer is based on the measurement of lights absorption and transmission through a sample across the ultraviolet and visible regions of the electromagnetic spectrum. The instrument typically uses two lamps (deuterium for UV and a tungsten-halogen for visible light) that together cover the full spectral range. A monochromator selects the desired wavelengths and scans through the spectrum by varying its position.

The monochromatic light beam is then split and directed towards both the sample and a reference path. As the light passes through the sample, its intensity is attenuated depending on the materials absorption characteristics. A photodetector compares the transmitted intensity to the reference, and the resulting signal is amplified and processed to generate transmission and absorption spectra [34].

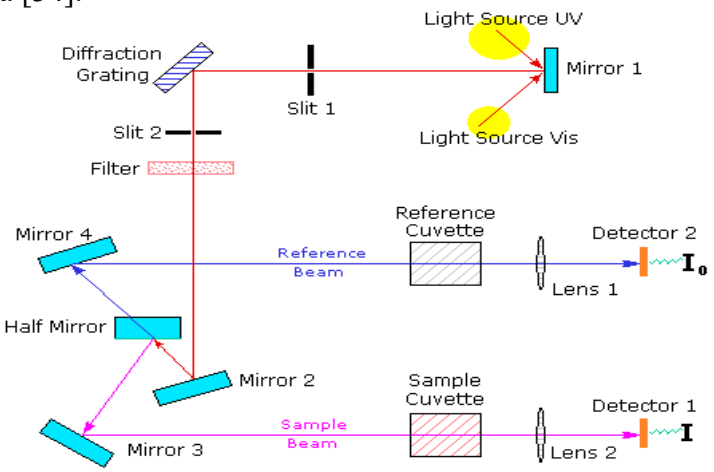

Figure II.12: Schematic Representation of a UV-Visible Spectrophotometer

In the present work, optical measurements were performed using a Perkin Elmer Lambda 950 UV-Vis spectrophotometer. Transmission and absorption spectra of the SnS: Mg thin films were recorded in the visible range to determine optical parameters such as bandgap energy, which is one of the important characteristics justifying the suitability of the material for optoelectronic and photovoltaic applications [33].

Figure II.13: Perkin Elmer Lambda 950 UV-Vis spectrophotometer

II.4.4. Electrical Characterization by Hall Effect

The Hall-effect electrical characterization technique was used to determine resistivity, type of conduction, carrier concentration, and mobility of charge carriers in our samples.

The basic physical principle on which this technique is based [Putley 1960] is the Lorentz force. When an electron moves under the influence of an electric field in a direction perpendicular to an applied magnetic field (B), it experiences a force perpendicular to the plane formed by its trajectory and B. For n-type semiconductors, the charge carriers are primarily electrons with a density N_H.

Consider an example of a rectangular semiconductor (Figure II.14). When a magnetic field B is applied perpendicular to the sample plane (in the z-direction), the negatively charged carriers experience the Lorentz force and deflect from the current path in the y-direction. The deflection of electrons causes an accumulation of charge on the sides of the sample, inducing a potential difference between the two sides of the sample [21].

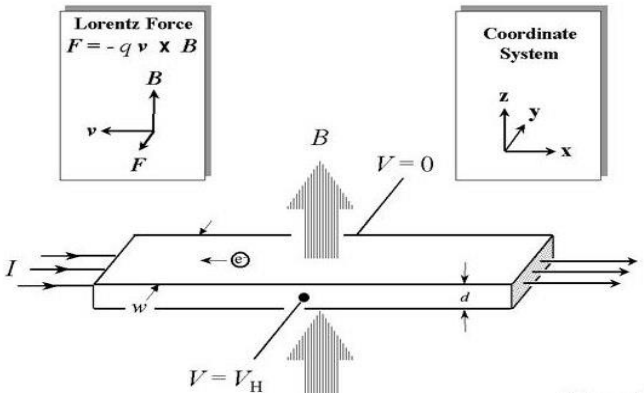

Figure II.14: Schematic Representation of the Hall Effect

This potential difference is called the Hall voltage (VH), and its magnitude is given by the equation:

$$V_H = I.\frac{B}{q.N_H.d} \quad \text{..... (II.3)}$$

where:

- q: is the charge of the electron,
- d: is thickness of the conducting layer.

In this study, the HMS-3000 Hall Effect Measurement System was used to measure the electrical properties of the SnS: Mg thin films. This system is equipped with high precision for determining the carrier concentration, mobility, and resistivity. The hall voltage is measured under conditions and data are analyzed to derive the required electrical characteristics of the samples [33].

Figure II.15: Setup of the HMS 3000 Instrument Used for Electrical Characterization.

II.5. SnS: Mg Films Prepared by Ultrasonic Spray Pyrolysis

The SnS: Mg thin films were synthesized using the Ultrasonic Spray Pyrolysis (USP) method, which is a chemical deposition method that uses an aqueous precursor solution converted to a fine mist. This mist is directed onto a heated substrate, where the chemical compounds decompose thermally and form a thin film. This technique is recognized for its simplicity, cost-effectiveness, and ability to produce uniform films with controlled composition [33].

II.5.1. Substrate Preparation

Glass substrates served as an undercoat for film deposition. Before deposition, the substrates underwent a very thorough cleaning protocol to get away with surface contaminants which might have adversely affected film quality and adhesion likely to affect quality of films and their adhesion to substrates. The cleaning was done through two main provisions:

- Degreasing of preventive measure with ethanol: The glass slides were suspended in ethanol and scrapped gently to get rid of any organic residues such as oils and greases.

- Final rinse with double-distilled water: High-purity distilled water wash eliminated any remaining inorganic impurities to avoid salt residues during drying.

This cleaning procedure ensured the substrates were chemically clean, suitable to allow even growth of films [33].

II.5.2. Precursor Solution Preparation

The deposition solution was prepared by dissolving the following components in 50 mL of distilled water:

- **Tin (II) chloride dihydrate ($SnCl_2 \cdot 2H_2O$)**: used at a concentration of 0.1 M, serving as the source of Sn^{2+} ions.

- **Thiourea ($CS(NH_2)_2$):** also used at a concentration of 0.1 M, acting as the source of S^{2-} ions necessary to form the SnS compound.

After both compounds were dissolved thoroughly in water then magnesium chloride dihydrate ($MgCl_2 \cdot 2H_2O$) was added into the same solution in varying proportions so as to incorporate magnesium into SnS matrix.

The magnesium doping levels were set at y=0%, 2%, 4%, 6%, and 8%, where y represents the molar ratio of Mg relative to Sn in the precursor solution. By varying the level of doping, we hoped to assess the impact of concentration of magnesium on the structural, optical, and electrical properties of the resulting SnS: Mg thin films [33].

The following figure illustrates the experimental steps taken to prepare the solution:

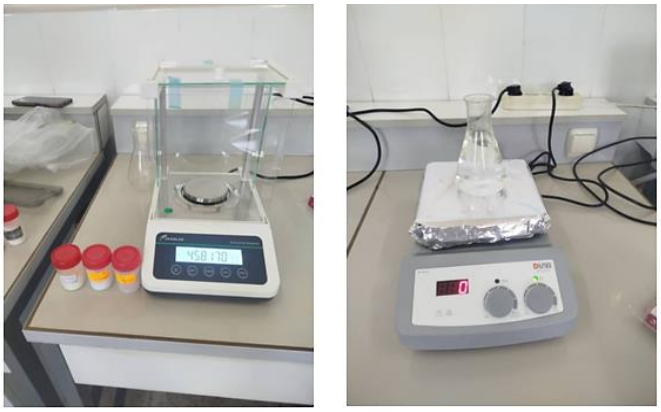

Figure II.16: Experimental steps for preparing the magnesium-doped precursor solution.

II.5.3. Ultrasonic Spray Deposition

Once the precursor solution was ready, it was loaded into the tank of the ultrasonic spray pyrolysis system. This system includes a vibrator operating at frequency of 40 kHz, which converts the liquid solution into fine and homogeneous mist composed of micron-sized droplets. This frequency is ideal for generation uniform droplets that allow for consistent film thickness and quality.

The mist was directed toward the glass substrates sitting on a hot plate held at a constant temperature of 350 degrees, which was sufficiently hot to ensure that thermal decomposition of the chemical species and formation of the SnS: Mg film on the substrate surface occurred.

During the deposition, the following parameters were maintained:

- **Spray time:** 30 minutes, providing sufficient time for a uniform and adequately thick films to form.

- **Nozzle-to-substrate distance:** 4.5 cm, carefully chosen to allow the droplets to reach the substrate without evaporating prematurely or dispersing irregularly.

These conditions especially the substrate temperature, solution concentration, spray time and nozzle distance were strictly controlled throughout the experiment as they significantly influence the resulting film's morphology, thickness and physical characteristics [33].

II.6. Conclusion

In this chapter, we examined the characterization and preparation of thin sulfide (SnS)thin films, focusing on their potential for photovoltaic applications. we began by explaining rational behind selection as an absorber material, based on its phase stability and favorable properties. The chapter then explored the optical, electrical, structural, and morphological characteristics of SnS, demonstrating its suitability for thin-film solar cells. Key experimental technique used for the investigation and characterization of SnS were discussed in detail, including ultrasonic spray pyrolysis (USP), X-ray diffraction (XRD), UV-visible spectrophotometry and Hall effect measurements. Finally, we described the step-by-step preparation of magnesium doped SnS (SnS: Mg) thin film using the USP technique.

References

[1] R. Herzenberg, Rev. Miner. 4 (1932) 33.

[2] M. Calixto-Rodriguez, H. Martinez, A. Sanchez-Juarez, J. Campos-Alvarez, A. Tiburcio-Silver, M.E. Calixto, Thin Solid Films 517 (2009) 2497–2499.

[3] S.K. Panda, A. Antonakos, E. Liarokapis, S. Bhattacharya, S. Chaudhuri, Materials Research Bulletin 42 (2007) 576–583.

[4] T. Jiang, G.A. Ozin, J. Mater. Chem. 8 (1998) 1099–1108.

[5] J.A. Andrade-Arvizu, M. Courel-Piedrahita, O. Vigil-Galan, " Structural and Electrical Properties of SnS Thin Films ", Mater. Sci.: Mater. Electron. (2015).

[6] W. Albers, C. Haas, H.J. Vink, J.D. Wasscher, Journal of Applied Physics 32 (1961) 2220–2225.

[7] S.C. Ray, M.K. Karanjai, D. DasGupta, Thin Solid Films 350 (1999) 72–78.

[8] L.A. Burton, D. Colombara, R.D. Abellon, F.C. Grozema, L.M. Peter, T.J. Savenije, G. Dennler, A. Walsh, Chem. Mater. 25 (2013) 4908−4916.

[9] T.H. Sajeesh, A.R. Warrier, C.S. Kartha, K.P. Vijayakumar, Thin Solid Films 518 (2010) 4370–4374.

[10] L.A. Burton, A. Walsh, J. Phys. Chem. C 116 (2012) 24262–24267.

[11] P. Woulfe, Philosophical Transactions, the Royal Society, London 61 (1771) 114–130.

[12] J.M. Skelton, L.A. Burton, A.J. Jackson, F. Oba, S.C. Parker, A. Walsh, Phys. Chem. Chem. Phys. 19 (2017) 12452–12465.

[13] C. Gao, H. Shen, L. Sun, Appl. Surf. Sci. 257 (2011) 6750–6755.

[14] E. Guneri, C. Ulutas, F. Kirmizigul, G. Altindemir, F. Gode, C. Gumus, Appl. Surf. Sci. 257 (2010) 1189–1195.

[15] C. Gao, H. Shen, L. Sun, Appl. Surf. Sci. 257 (2011) 6750–6755.

[16] V. Robles, J.F. Trigo, C. Guillén, J. Herrero, J. Mater. Sci. 48 (2013) 3943–3949.

[17] B.G. Jeyaprakash, R. Ashok Kumar, K. Kesavan, A. Amalarani, American Science 6 (2010) 22–26.

[18] S. Cheng, G. Conibeer, Thin Solid Films 518 (2011) 5.

[19] B. Subramanian, C. Sanjeeviraja, M. Jayachandran, Mater. Chem. Phys. 71 (2001) 40–46.

[20] P. Lu, H. Jia, Y. Yang, S. Cheng, Semiconductor Photonics Technol. 1007 0206 (2010) 04-0132-05.

[21] K. Kamli, Mémoire de magister, " Elaboration et caractérisations physico-chimiques des couches minces de sulfure d'étain par spray ultrasonique : Effet des sources d'étain ", (2013).

[22] M. Cruz, J. Morales, J.P. Espinos, J. Sanz, Solid State Chem. 175 (2003) 359–365.

[23] E. Guneri, F. Gode, C. Ulutas, F. Kirmizigul, G. Altindemir, C. Gumus, Chalcogenide Lett. 7 (2010) 685–694.

[24] H.K. Park, J. Jo, H.K. Hong, G.Y. Song, J. Heo, Curr. Appl. Phys. 15 (2015) 964–969.

[25] N. Koteeswara Reddy, K.T. Ramakrishna Reddy, Solid-State Electron. 49 (2005) 902–906.

[26] A. Bougrine, A. El Hichou, M. Addou, J. Ebothé, A. Kachouna, M. Troyon, Mater. Chem. Phys. 80 (2003) 438–445.

[27] Y. Ahmed Memdouh, Mémoire de magistere, " Elaboration et caractérisation des couches minces CuInSe2 par électrodéposition (Effet de recuit) ", Université Ziane Achour - Djelfa, (2015).

[28] A. Bouzidi, Mémoire de master académique, " Etude de l'influence du dopage sur les propriétés structurales et optiques des nanostructures d'oxyde de zinc élaborées par la technique sol-gel ", Université Mohames Boudief - M'sila, (2017).

[29] F. Yniheb, Mémoire de magistère, " Contribution à l'élaboration des couches minces d'oxydes transparents conducteurs (TCO) ", Université Mentouri Constantine, (2010).

[30] S. Rahmane, Mémoire de Doctorat, " Élaboration et caractérisation de couche mince par spray et pulvérisation magnétron ", Université Mohamed KH eider - Biskra, (2008).

[31] M. Messoudi, Thèse de doctorat, " Elaboration et caractérisation de couches minces SnS ", Université des Frères Mentouri Constantine, (2016).

[32] K.H. Bouchoureb, Mémoire de magister, " Elaboration et caractérisation des couches minces $CuInS_2$ ", Université d'Oran Sciences et Technologie Mohamed Boudiaf, (2015).

[33] Z. Hadef, K. Kamli, A. Akkari, H. Hadjoudja, N.T. Kamoun, O. Kamli, A. Djarmoune, F. Ait Merzeg, J. Mater. Sci.: Mater. Electron. 35 (2024) 1632.

[34] F.A. Settle, Handbook of Instrumental Techniques for Analytical Chemistry, Prentice Hall, U.S.A, (1997).

Chapter III:
Results and discussions

III.1. Introduction

Chalcogenide materials have been major role in the field of photovoltaic devices due to its exciting opto-electrical properties [1, 2]. SnS thin films are specially candidate as absorber layer in the construction of solar cells technology [3–4], owing to their orthorhombic structure [3] band gap in range of 1.3 to 1.7 eV [5] and high absorption coefficient in visible region (~ 105 cm $^{-1}$). SnS thin film has been synthesized by various methods like ultrasonic spray pyrolysis [6–7]. Doping of semiconductors with transition metal ions is very essential for electronic and optoelectronic applications. When SnS is doped with Magnesium impurities, Sn^{2+} ions are replaced by (Mg^{2+}) ions which improve the optoelectrical properties. This chapter presents the effect of Mg incorporation on the structural, optical and electrical properties of SnS thin films synthesized by USP and annealed at 350 °C.

III.2. Structural analysis

XRD pattern of pure and SnS: Mg thin films (2%, 4%, 6%, and 8%) are shown in Figure III 1. SnS growth looks to be crystalline. The SnS thin films exhibit an orthorhombic crystalline structure, with a high orientation along the (130) direction.

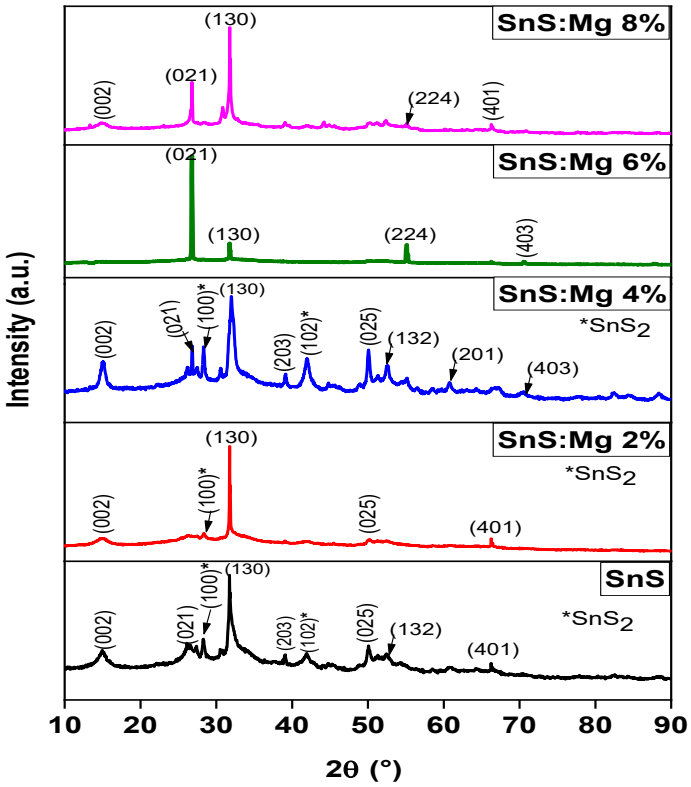

Figure III.1: XRD patterns of pure and SnS: Mg thin films

For the prepared thin films using 0%, 2% and 4% of Mg, it can be observed the presence of two phases SnS_2 and SnS. Peaks of SnS_2 with (100) and (102) matching planes were detected

at 2θ values of 28.20◦, and 41.88◦, respectively, these findings correspond to file numbers JCPDS 23-0677.

Peaks corresponding to SnS_2 were observed at 2θ values of 28.20° and 41.88°, matching the (100) and (102) planes, respectively, consistent with JCPDS 23-0677 data. Hence, with higher Mg incorporation levels (6% and 8%), all reflections can be attributed to the pure orthorhombic SnS phase associated to JCPDS 01-079 2193 data. There is an absence of peaks corresponding to other SnS phases, suggesting the formation of pure SnS thin films.

The values the diffracting angles are 26.36◦, 55.13◦, 66.33◦, and 70.56◦, respectively, with corresponding planes (021), (130), (224), (401), and (403). However, with the increase in Mg incorporation concentration from 4 to 6%, the preferred orientation change, due to the deteriorated of the secondary phase (SnS_2), leading to a higher predominance of the SnS pure phase. The Mg doping can also lead to changes in the peak shifting and intensity of diffraction peaks [8].

Therefore, the shift in the diffraction peak position of SnS in response to Mg doping aligns with Vegard's law, indicating that the presence of Mg atoms has induced an assessable change in the lattice parameters of the SnS crystal structure [9].

This observation further supports the successful incorporation of Mg dopant cation into the SnS lattice and underscores the structural modifications induced by doping without the formation of secondary phases SnS_2. Hence the substitution of smaller dopant ions, like Mg^{2+} (65 pm), for larger host ions, such as Sn^{2+} (118 pm), leads to lattice distortion due to the disparity in ionic sizes [10].

This distortion alters the interatomic distances within the crystal lattice, consequently causing a shift in the diffraction peaks position in the XRD pattern.

Furthermore, Mg incorporation can influence the growth and alignment of crystalline domains within SnS thin films, leading to enhancements in their structural properties. The incorporation of Mg^{2+} dopant ions, into the SnS lattice can promote better layer alignment and crystalline quality by reducing lattice defects, enhancing grain growth, and improving the overall structural coherence of the material. Indeed, the data suggest that increasing the doping concentration above 4% enhances the crystalline quality of the film. Specifically, a notable increase in peak intensity at 6% SnS: Mg indicates that the film possesses high crystalline quality.

Debye–Scherrer formula [11] relates the broadening of diffraction peaks in the XRD pattern to the crystal lite size (D) of the SnS material is given by:

$$D = \frac{K\lambda}{\beta cos\theta} \ldots\ldots\ldots\ldots \text{(III.1)}$$

where:

- K is the shape factor (typically taken as 0.94 for isotropic crystals).
- λ is the wavelength of the X-ray radiation used (usually CuKα radiation with λ = 1.5406 Å).
- β is the full-width at half maximum (FWHM) of the diffraction peaks.
- θ is the Bragg angle of the highest diffraction peak.

Williamson and Smallman's formula [12] for determining dislocation density (δ) of deposited SnS: Mg thin films is typically expressed as:

$$\delta = \frac{1}{D^2} \ldots\ldots\ldots\ldots \text{(III.2)}$$

The relation for estimating micro strain (ε) developed in the synthesized SnS: Mg samples in materials is often given as [13]:

$$\varepsilon = \frac{\beta cos\theta}{4} \ldots\ldots\ldots\ldots \text{(III.3)}$$

Hence, Table III.1 containing the results for microstructural parameters as show in table below.

Mg doping atomic percentage (at. %)	Thickness (nm)	Crystallite size (D) nm	Dislocation density (δ)×10^{-4} (lines. nm^{-2})	Micro strain (ε) × 10^{-4}
0	652	108	0.86	3.22
2	655	81	1.54	4.304
4	625	54	3.42	6.41
6	673	90	1.23	3.53
8	698	90	1.24	3.5

Table *III.1: Microstructural parameters of pure and SnS: Mg thin films*

Furthermore, the crystallite size and micro strain are shown in Figure.III.2 The real crystal atomic arrangement deviates locally from the ideal crystal structure due to the presence of defects in the crystal structure.

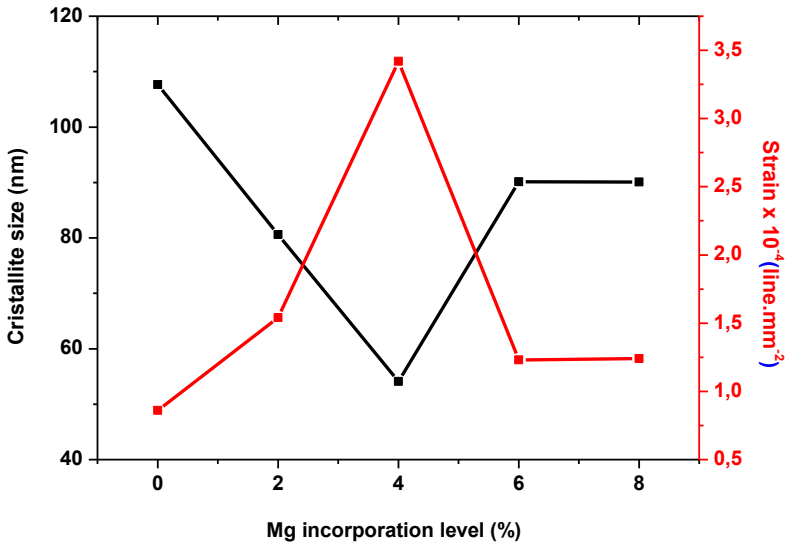

Figure III. 2:Variation of crystallite size and Strain of pure and SnS: Mg thin films

According to the Figure III.2 it can be noticed that the micro strain increase with Mg incorporation increasing from 0 to 4%, which implies a falling in crystallite size leading to a deterioration in the film's crystallinity. Nonetheless, with increasing Mg incorporation to 6% and 8%, the crystallinity increases to 90 nm, though the micro strain decreases to 3.53×10^{-4}. Additionally, the increase in crystallinity could be attributed to the enhanced crystal growth facilitated by Mg incorporation. When Mg atoms are incorporated into the SnS lattice, they may aid in stabilizing the crystal structure and promoting the growth of larger crystallites associated with a potentially reducing the formation of defects such as dislocations [14]. The reduction in micro strain values observed when the incorporation of Mg is above 4% suggests several effects on the crystallinity of the samples.

III.3. Optical analysis

The optical properties of Mg-doped SnS thin films were systematically investigated through transmittance and band gap within the wavelength range of 350–800 nm. These analyses reveal critical insights into the influence of Mg incorporation on the optical behavior of the films.

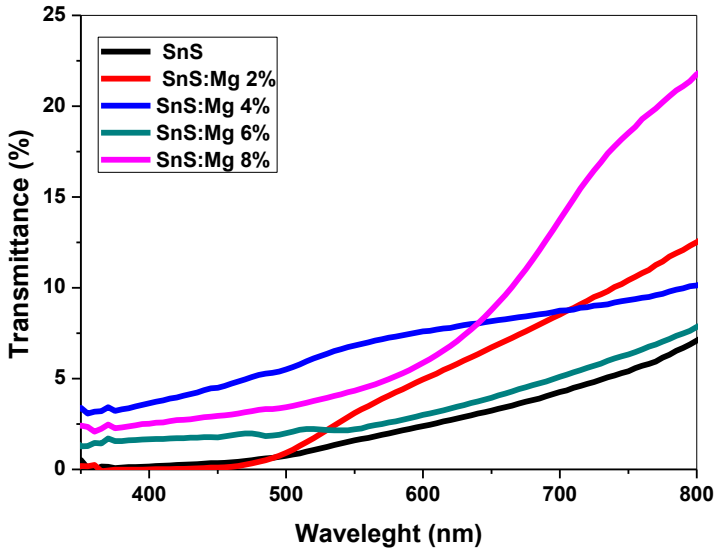

Figure III.3: Transmission spectra of SnS :Mg samples

Figure III.3 showing the transmittance spectra provided information about the amount of light transmitted through the SnS :Mg films in the range of 350 – 800 nm. An increase in transmittance with increasing incident wavelength suggests a trend where the Mg-doped SnS film becomes more transparent at longer wavelengths. The transparency is less for 6% SnS: Mg film comparing to other concentrations (2%, 4% and 8%) except the pure film. The decrease in transmittance of 6% SnS: Mg sample may be caused by the Mg/Sn ratio increases accompanied also by an increasing in carrier concentration.

It seems that the SnS: Mg films, except for those with an 8% Mg incorporation concentration, exhibit an average optical transmittance of approximately 10%. This suggests that these films may be suitable for photovoltaic applications as a good absorber.

Therefore, it can be concluded that all films irrespective of the Mg incorporation level employed are absorbent in the visible range (400-750 nm) of the optical spectrum, reaching values of transmittance less than 8% at 550 nm. The increase of transmittance at higher Mg incorporation levels (>4 at. %) may be attributed to the decreased scattering of photons by crystal defects created by doping. The free carrier absorption of the photons may also contribute to the observed increasing in the optical transmission of heavily Mg incorporation films. It is worth noting here that the 6 at. % represents the optimum Mg incorporation concentration.

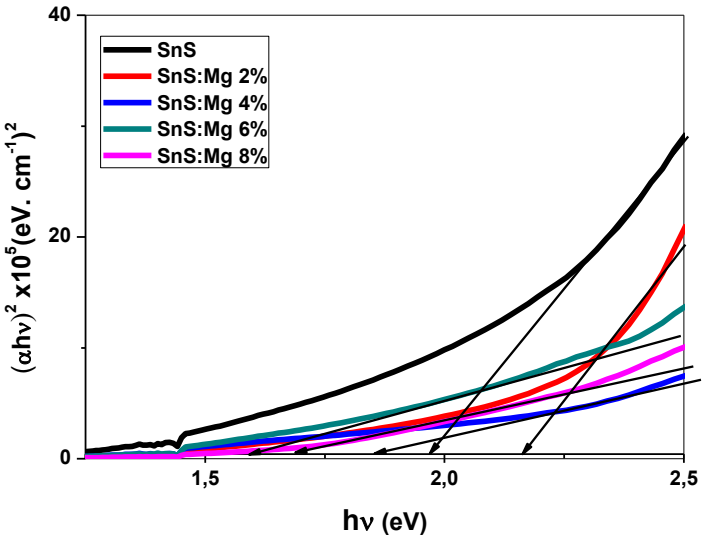

Figure III.4: Variation of $(\alpha h\nu)^2$ as a function of the photon energy (hν).

Figure III.4 represents typically plot for pure SnS film yields an optical band gap of 1.96 eV. For pure SnS, optical band gap is obtained 1.96 eV. Doping SnS with Mg impurities has a significant impact on its optical band gap. It is decreased from 2.16 eV to 1.59 eV with Mg incorporation concentration increasing from 2 to 6% and then increased to 1.68 eV for 8 at.%.

This significant decrease in band gap of SnS when the Mg at. % increase indicates that it is more conducive to absorbing lower-energy photons, which indicates an improvement in crystallinity [15, 16]. However, as the Mg incorporation concentration increases beyond 6%, the band gap stabilizes and even slightly increases at 8 at.%.

The incorporation of 6% Mg impurities in the SnS film, results in a lower band gap of 1.59 eV. Achieving a band gap, especially through doping, can have significant implications for the material's properties and potential applications [17, 18].

III.4. Electrical properties

The Electrical properties of pure and SnS: Mg thin films is determinated by using Hall Effect measurement system, it is an important test in the photovoltaic field to determine its maximum benefit in solar energy conversion. The influence of the Mg incorporation on electrical proprieties of SnS matrix has been investigated based on the study of resistivity, conductivity, Hall mobility, carrier density, and the conductivity type of the films, the obtained results were listed in Table.III. 2, and the variation of resistivity and conductivity values with respect to Mg incorporation is clearly illustrated in FigureIII.5.

Table *III.2: Summarizes values of electrical proprieties of pure and SnS: Mg thin films*

Mg incorporation percentage (at. %)	Resistivity (Ω.cm)	Conductivity ($\Omega^{-1}.cm^{-1}$)	Mobility (cm^2/Vs)	Carrier density (cm^{-3})	Type cond.
0 (Pure)	5.34×10^{2}	1.87×10^{-3}	5.12	2.25×10^{15}	P
2	2.11×10^{1}	4.73×10^{-2}	7.21	4.10×10^{16}	P
4	2.20×10^{-1}	0.45×10^{1}	17.23	1.61×10^{18}	P
6	1.58×10^{-2}	6.33×10^{1}	21.54	1.47×10^{19}	P
8	1.83×10^{-1}	1.54×10^{1}	16.76	1.02×10^{18}	P

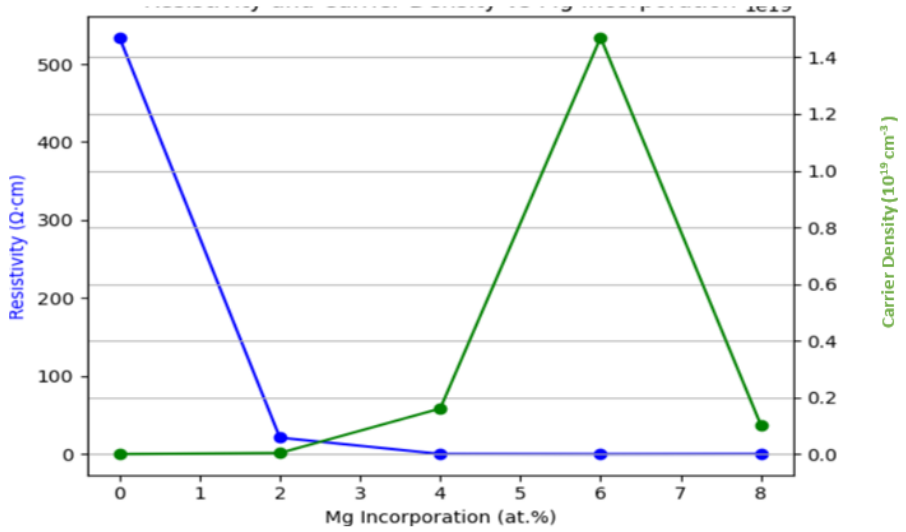

Figure III.5: Variation of Resistivity and Conductivity with Mg Incorporation in SnS Thin Films

Hall Effect measurements are indeed crucial for understanding the electrical properties of materials, including thin films like pure and SnS: Mg. These measurements provide valuable insights into parameters such as resistivity, conductivity, carrier density, mobility, and even the type of conductivity exhibited by the films. Comparing these obtained results summarized in Table III.2, the impact of Mg incorporation on the electrical properties of the material can be assed. This information is vital for optimizing the performance of SnS thin films in photovoltaic applications, aiming for improved solar energy conversion efficiency.

A Significant decrease in the electrical resistivity of SnS: Mg films was revealed due to the substitution of Mg ions with SnS. It achieves a minimum at 1.58×10^{-2} Ω.cm for 6% Mg incorporation, whereas the higher conductivity value observed at 63.3 Ω^{-1} cm^{-1} which caused by the improvement in the grain size in accordance with XRD results. In addition, the carrier

con centration depicts a considerably increased attains a maximum at 1.47×10^{19} cm^{-3} for 6% Mg incorporation due to addition of Mg impurities into SnS matrix. Also, similar behavior was presented in Hall mobility at the same Mg incorporation percentage with obtained values of 21.54 cm^2/Vs. Confirming p-type conductivity from Hall measurements of pure and SnS: Mg films indicates that the holes are the majority charge carriers in these materials.

III.5. Conclusion

The synthesis and characterization of pure and SnS: Mg thin films deposited by spray pyrolysis under different Mg incorporation concentration (2%, 4%, 6% and 8%) have been investigated. Structural analysis identified that the grown films have an orthorhombic crystal structure which clearly affected by the incorporation of Mg impurities into SnS matrix. In addition, optical studies presented the visible region transmittance of synthesized films and showed the low band gap value of 1.59 eV for optimized incorporation con centration. The Hall Effect measurements presented the low resistivity of 1.58×10^{-2} Ω cm with high mobility of 21.54 cm^2/Vs and very high carrier concentration of 1.47×10^{19} cm^{-3} for 6 wt.% of SnS: Mg thin film. These findings confirm that the 6% Mg-doped SnS thin film exhibits promising properties for photovoltaic applications.

References

[1] M. Buffière, D.S. Dhawale, F. El Mellouhi, "Chalcogenide materials and derivatives for photovoltaic applications", Energ. Tech., 7(11) (2019) 1900819.

[2] R. Mariappan, T. Mahalingam, V. Ponnuswamy, "Preparation and characterization of electrodeposited SnS thin films", Optik, 122 (2011) 2216–2219.

[3] S.C. Ray, M.K. Karanjai, D. DasGupta, "Structure and photoconductive properties of dip-deposited SnS and SnS_2 thin films and their conversion to tin dioxide by annealing in air", Thin Solid Films, 350 (1999) 72–78.

[4] A.R. Garcia-Angelmo, M.T.S. Nair, P.K. Nair, "Evolution of crystalline structure in SnS thin films prepared by chemical deposition", Solid State Sci., 30 (2014) 26–35.

[5] J.A. Andrade-Arvizu, M.F. García-Sánchez, M. Courel Piedrahita, J. Santoyo-Morales, D. Jiménez-Olarte, M. Albor-Aguilera, O. Vigil-Galán, "Pressure induced directional transformations on close spaced vapor transport deposited SnS thin films", Mater. Design., 110 (2016) 878–887.

[6] Z. Hadef, K. Kamli, O. Kamli, S. Labiod, "Effect of substrate temperature on physical properties of Co doped SnS_2 thin films deposited by ultrasonic spray pyrolysis", Chalcogenide Lett., 20(8) (2023) 587–597.

[7] K. Kamli, Z. Hadef, O. Kamli, B. Chouial, M.S. Aida, H. Hadjoudja, S. Labiod, "Effect of deposition time on the properties of CuxZnyS thin films synthesized by ultrasonic spray pyrolysis", J. Nano Res., 81 (2023) 37–52.

[8] L. Amalraj, C. Sanjeeviraja, M. Jayachandran, "Spray pyrolysised tin disulphide thin film and characterisation", J. Cryst. Growth, 234 (2002) 683–689.

[9] B. Zhou, S. Li, W. Li, J. Li, X. Zhang, S. Lin, Z. Chen, Y. Pei, "Thermoelectric properties of SnS with Na-doping", ACS Appl. Mater. Interfaces, 9(39) (2017) 34033–34041.

[10] S.H. Chaki, M.D. Chaudhary, M.P. Deshpande, "Effect of indium and antimony doping in SnS single crystals", Mater. Res. Bull., 63 (2015) 173–180.

[11] B.H. Baby, D.B. Mohan, "The effect of in-situ and post deposition annealing towards the structural optimization studies of RF sputtered SnS and Sn2S3 thin films for solar cell application", Sol. Energy, 189 (2019) 207–218.

[12] L.I. Maissel, R. Glang, P.P. Budenstein, "Handbook of thin film technology", Electrochem. Soc., 118 (1971) 114C–118C.

[13] A. Rmili, L. Soussi, R. Jdaa, T. Garmim, C. Louardi, A. El Bachiri, A. Louardi, A. Talbi, K. Nouneh, M. Mabrouki, H. Erguig, "Cu doped SnS thin films deposited by the spray method: characterization and numerical simulation using SCAPS-1D", Opt. Quantum Electron., 55 (2023) 424.

[14] S. Sebastian, I. Kulandaisamy, S. Valanarasu, I.S. Yahia, H.S. Kim, D. Vikraman, "Microstructural and electrical properties evaluation of lead doped tin sulfide thin films", J. Sol-Gel Sci. Technol., 93 (2020) 52–61.

[15] J. Tauc, R. Grigorovici, A. Vancu, "Optical properties and electronic structure of amorphous germanium", Phys. Status Solidi B, 15 (1966) 627–637.

[16] A.M.S. Arulanantham, S. Valanarasu, A. Kathalingam, K. Jeyadheepan, "Solution volume effect on structural, optical and photovoltaic properties of nebulizer spray deposited SnS thin films", J. Mater. Sci.: Mater. Electron., 15 (2018) 12899–12909.

[17] S. Gedi, V.R. Minnam Reddy, C. Park, J. Chan-Wook, K.T. Ramakrishna Reddy, "Comprehensive optical studies on SnS layers synthesized by chemical bath deposition", Opt. Mater., 42 (2015) 468–475.

[18] A. Javed, Qurat-ul-Ain, M. Bashir, "Controlled growth, structure and optical properties of Fe-doped cubic π-SnS thin films", J. Alloys Compd., 759 (2018) 14–21.

General Conclusion

General Conclusion

This study has explored the synthesis and characterization of the magnesium doped of tin sulfide (SnS: Mg) thin films with a view to their application in photovoltaic devices. Beginning with a foundational review of photovoltaic technology and thin-films deposition methods, we established a clear understanding of the principles and mechanisms underlying the photovoltaic effect , along with the pivotal role of thin-film materials in enhancing solar cell performance .A comparative analysis of physical and chemical deposition methods highlighted the advantages of ultrasonic spray pyrolysis (USP) as an effective , low-cost technique for fabricating semiconducting thin films .

Building upon this theoretical foundation, we examined the specific properties of SnS as a promising absorber layer, due to its favorable optical bandgap, phase stability and environmental compatibility. The comprehensive study of its structural, optical and electrical characteristics demonstrated its high potential for integration into next-generation solar cells. We then extended the investigation to Mg-doped SnS thin films, focusing on variation in doping concentration to optimize material performance.

The experimental results revealed that the incorporation of mg significantly influenced the structural orientation, optical absorption, and electrical conductivity of SnS thin films. In particular, the films doped 6% Mg exhibited optimal properties, including low resistivity, high carrier mobility, and a narrow bandgap, all of which are crucial foe efficient photovoltaic conversion.

Finally, this work contributes valuable insights into cost-effective, non-toxic, and high-performance absorber materials for thin -film solar cells. The findings confirm that SnS :Mg, particularly at optimized doping levels, holds great promise as a candidate for future photovoltaic applications.